THE ROLE OF ANTEROGRADE IFT MOTORS AND LIPID SCRAMBLASES IN THE ORGANIZATION OF EXTRACELLULAR VESICLE CARGO INTO CILIARY MICRODOMAINS

by

Rachael M. Gill

A dissertation submitted to the Faculty of the University of Delaware in partial fulfillment of the requirements for the degree of Master of Science in Biological Sciences

Spring 2022

THE ROLE OF ANTEROGRADE IFT MOTORS AND LIPID SCRAMBLASES IN THE ORGANIZATION OF EXTRACELLULAR VESICLE CARGO INTO CILIARY MICRODOMAINS

by

Rachael M. Gill

Approved: ______________________________

Jessica Tanis, Ph.D.
Professor in charge of thesis on behalf of the Advisory Committee

Approved: ______________________________

Velia Fowler, Ph.D.
Chair of the Department of Biological Sciences

Approved: ______________________________

John A. Pelesko, Ph.D.
Dean of the College of Arts and Sciences

Approved: ______________________________

Louis F. Rossi, Ph.D.
Vice Provost for Graduate and Professional Education and
Dean of the Graduate College

ACKNOWLEDGMENTS

I would like to express sincere gratitude to the entire Tanis lab for their support in my research. First, to Dr. Tanis, who has consistently supported and encouraged me. I am so grateful that I was able to work under her mentorship and guidance. Next, I would like to express thanks to Mike for laying all the groundwork for the EV project, training me, and being my sounding board when I couldn't figure something out. I'd like to thank Andy for always being willing to help no matter what, reteaching me things when I forgot them, for repeatedly unlocking the door to lab or the cubby when I couldn't find my keys, and being a great friend. I am so appreciative of all of my past and current lab members – Ime Nkanta, Malek Elsayyid, Denis Touroutine, Kirsten Kervin, Katherine Wagner, Jackie Littman, Erin Smith, Charlotte Leslie, Carter O'Brien, John Salsini-Tobias, Allison Davis – for all the help and making working in the Tanis lab a joy. I also would like to thank my committee members, Dr. Selva and Dr. Jaramillo-Lambert, for their support and feedback in my research. I would also like to acknowledge the important contribution of the Delaware Bioimaging Center staff, especially Dr. Caplan and Dr. Le Marchand, for training me in how to use the microscopes and image analysis software. I am very grateful to the University of Delaware and the Biological Sciences department for providing me with the opportunity to conduct my research, and to the CBI program for providing funding for part of my time here. Finally, I would like to thank my husband, Taylor, and my family for their support as I would not have been able to complete this research without them in my corner.

TABLE OF CONTENTS

LIST OF TABLES

LIST OF FIGURES

ABSTRACT

Extracellular vesicles (EVs) are lipid enclosed containers of signaling molecules, metabolic products, various proteins and RNAs that play a wide variety of roles in cellular processes. Although they are likely released from most cell types, the mechanisms underlying extracellular vesicle (EV) cargo sorting and biogenesis have not yet been fully elucidated due in part to the reliance in the field on *in vitro* models. Utilizing a *C. elegans* ciliated sensory neuron EV model that releases two separate subpopulations of EVs containing either CLHM-1::tdTomato or PKD-2::GFP, we were able to shed light on a possible sorting mechanism via physical separation of EV cargo into domains within the cilia. Intraflagellar transport (IFT) is required for construction of the middle and distal ciliary segments, proper protein localization, and EV release. Anterograde IFT motors OSM-3 and KLP-11 are required for the normal release of PKD-2 containing EVs, but not CLHM-1 containing EVs. Anterograde IFT is also required for proper localization of PKD-2 in the distal segment of the cilia, and abundance of CLHM-1 within the periciliary membrane compartment. The transition zone, which separates the cilia proper from the periciliary membrane compartment, is also required for normal EV subpopulation abundance. Transition zone breakdown caused by *mks-5* and subsequent disorganization of proteins within the cilia correlates with an increase in colocalized EVs containing both CLHM-1::tdTomato and PKD-2::GFP.

The *C. elegans* EV model can be used to study the impact of Ca^{2+} on EV biogenesis. Addition of the calcium ionophore ionomycin corresponded with an

increased release in CLHM-1 containing EVs. This calcium-induced release of CLHM-1 containing EVs may occur via the scramblase ANOH-1. Scramblases are hypothesized to play a role in EV biogenesis by inducing membrane curvature in response to a chemical signal, such as calcium influx. In *C. elegans, anoh-1* mutants release significantly fewer CLHM-1 containing EVs when compared to WT. Preliminary data indicates that biogenesis of the PKD-2::GFP containing subpopulation does not required ANOH-1. Further investigation is needed into the role of calcium in EV biogenesis.

Chapter 1

INTRODUCTION

1.1 Extracellular Vesicles

Extracellular vesicles (EVs) contain cytosolic proteins, mRNAs, miRNAs, and metabolic products, surrounded by a heterogeneous bilayer enriched in lipids and membrane associated proteins [1–3]. Released from most if not all cell types, EVs can radically influence the functionality of target cells under physiological and pathological conditions, to maintain or alter homeostasis [3–5]. Currently, basic biological processes behind EV biogenesis and cargo sorting are poorly understood due to in part to limited opportunities for *in vivo* studies.

When first discovered in the 1940s, researchers mistakenly considered EVs released from the plasma membrane to be simply "cellular debris" [6]. This changed in 1977, when De Broe et al. showed EVs aiding in membrane turnover dynamics in intestinal cells [6,7]. Since then, EVs have been found to be released from all major cell types - including fibroblasts, blood cells, neurons, cancer cells, immune cells, epithelial cells and stem cells – and are now understood as playing a critical role in cellular communication and homeostasis [8,9]. Cell culture studies of mammalian cells have demonstrated that EV shedding can alter the size of primary cilia, playing a critical role in receptor shedding [10,11].

Shed EVs may exert their influence on target cells and cellular environments in various ways. Membrane associated proteins in EVs may act as a ligand for membrane receptors in target cells, triggering endocytosis [12,13]. Direct fusion of EVs with the plasma membrane (PM) has also been observed as lipids and transmembrane proteins within the EV membrane are readily incorporated into the bilayer of the receiving cell, altering membrane transport and dynamics [12–14]. Upon entering the cytosol of the target cell, protein cargo may bind to cytosolic receptors kickstarting or inhibiting signaling cascades or exhibit enzymatic functions on metabolites[1]. Additionally, mRNA cargo may be translated into functional proteins while inhibition of translation can be carried out by miRNAs[13]. EVs also function to remove unwanted contents from the cell of origin, seen most notably in shedding of channels and in membrane repair [10,13,15,16].

1.1.1 Types of EVs

EVs are categorized into three groups based on their mechanism of formation and size – apoptotic bodies, exosomes, and microvesicles [8,13,17–19]. Produced through membrane blebbing, apoptotic bodies, which are approximately 400-3000nm in diameter, contain cellular contents from the dying cell that are destined for destruction by macrophages. Exosomes, which are the smallest class of EVs at 30-100nm in diameter, are released when multivesicular bodies formed from late endosomes fuse with the PM, simultaneously releasing multiple EVs into the extracellular environment [20]. The final EV category, microvesicles (MVs), which are also known as ectosomes or microparticles, form from directed budding of the PM. MVs tend to be larger than exosomes, ranging from 50-200 nm in diameter [19].

1.1.2 EVs in physiological and pathophysiological processes

EVs were initially discovered within the blood [6,21]. Distinct MV subpopulations released from erythrocytes, platelets, and endothelial cells aid coagulation via tissue factor dependent and independent pathways [22–24]. In atherosclerosis, EVs released from cells undergoing shear stress promote inflammatory markers in the blood and activate cellular adhesion [22,25].

In the kidneys, EVs are released from tubular epithelium into the urine and play a role in paracrine signaling [9]. Fluorescently tagged EVs released from the proximal tubule can be absorbed into the distal tubule and collecting ducts within the same nephron, signaling an increase in aquaporin membrane insertion [26]. Alterations in EV cargo sorting and increased EV release have been observed during kidney ischemia [9]. In human kidneys, polycystin containing EVs are released, received by, and integrated into epithelial cell cilia, but this process is altered in autosomal dominant polycystic kidney disease[27,28].

Neurons and nervous system support cells also release EVs that serve a variety of purposes [29]. Evidence suggests that EVs shed from neurons could function to remove excess receptors or decrease gene silencing through miRNA release, regulating depolarization and protein production [30]. EVs are involved in the progression of neurodegenerative diseases. PrP^{C}, a prion precursor, has been found in the membranes of EVs derived from cerebral spinal fluid, while disease causing prions are EV cargo and act to upregulate EV biogenesis mechanisms [31]. Other misfolded proteins such as Tau and amyloid beta have been identified as EV cargo, although it has not been determined if EVs are acting in a protective capacity to shed toxic proteins or functioning pathologically to spread disease from cell to cell [31].

EVs also play a major role in the progression of cancer, including angiogenesis and immune evasion [32–40]. Cancer derived EVs often exert their effects locally, altering the cellular matrix, weakening the immune responses, and altering normal cellular signaling in the metastatic niche[33].

In clinical diagnosis and treatment, EVs offer many exciting possibilities. EV cargoes are reflective of cell of origin. Since EVs are present in easily accessible biological fluids, including urine, breastmilk, semen, saliva, blood, bile, and cerebrospinal, this suggests that EVs could be used as diagnostic markers of disease [8,41,42]. Additionally, liposomes, modelled after human EVs, can be utilized in cell targeted drug delivery. Recent treatments using “barcoded nanoparticles” delivered by liposomes, allows for clinicians to determine which specific combinations of a cocktail of chemotherapeutic drugs would be most effective in treating complex metastatic tumors in a patient-specific way [43]. Significant need persists for further research into mechanisms of EV biogenesis and cargo sorting to support the development of such diagnostic and treatment tools.

1.2 Microvesicle Biogenesis

Because the model utilized in this particular research releases microvesicles into the external environment (MVs), the remainder of this paper focuses on this EV subtype. While mechanisms are incompletely understood, a current consensus exists about the general steps of MV biogenesis **(Figure 1)**.

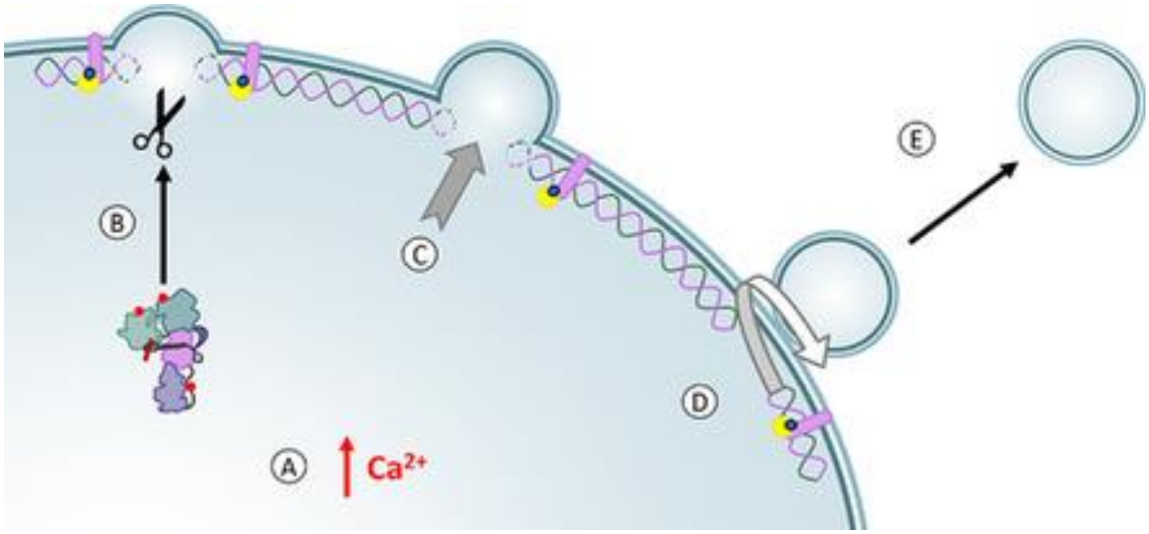

Figure 1: Steps of microvesicle biogenesis. (A) An increase in calcium initiates MV biogenesis. (B) Proteases such as calpains sever ties between the PM and the cytoskeleton. (C) Lipid translocases alter PM lipid composition. (D) Contractile proteins pinch off the MV. (E) MV is released. Figure adapted from Taylor & Bebawy, 2019.

First, remodeling must occur, disrupting anchorages tethering the plasma membrane to the cytoskeleton. Second, plasma membrane lipid asymmetry changes promote curvature of the PM as larger, conical shaped phospholipids such as phosphatidylserine (PS) and phosphatidylethanolamine (PE), flip to the outer leaflet. Lastly, contractile, scission, and cytoskeletal proteins act adjacent to the forming vesicle to promote its budding. Many of the individual players involved in this process have yet to be characterized, but new information is emerging that suggests a critical role of Ca^{2+} [45].

Ca^{2+} can induce vesiculation in various cell types, although the mechanism by which this occurs has not fully been elucidated [46] **(Figure 2)**. Ca^{2+} control of MV release is now being considered as a possible signal factor initiating all steps of MV biogenesis. Localized influxes of Ca^{2+}, referred to as “calcium sparks”, accomplished by the PM Ca^{2+} channel TRPM7, results in calpain activation [47]. Calpains are ubiquinone cysteine proteases that disassemble connections between the plasma membrane and cytoskeleton [41,48]. This activation has a localized effect, inducing vesiculation from the specific microdomain where the calcium spark occurred [47]. Increased calpain activity is associated with increased MV release from malignant cells which can be blocked by use of a calpain inhibitor such as calpain inhibitor II (ALLM) [49].

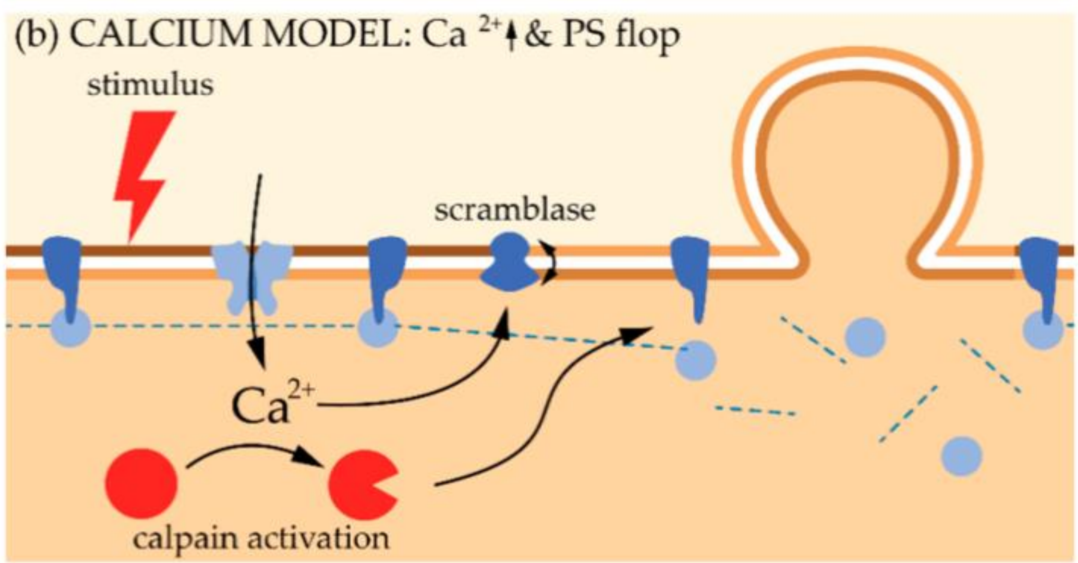

Figure 2: The hypothesized role of calcium in MV biogenesis. Calcium targets calcium-dependent translocases, calpains, and cytoskeleton proteins to enable MV biogenesis. Figure adapted from Pollet et al., 2018.

Localized Ca^{2+} influx may also play a role in lipid translocation in MV biogenesis. Under normal conditions, the inner leaflet of the PM contains high amounts of PS and PE, while the outer leaflet displays phosphatidylcholine (PC), phosphatidylinositol (PI), and glycolipids [50,51]. This distribution is maintained by the action of lipid translocases. ATP-dependent amino translocases flippases and floppases move PS and PE from the outer to the inner leaflet and move PC and other lipids to the outer leaflet, respectively [45]. Scramblases are Ca^{2+}-dependent translocases that can move lipids in either direction [52]. Interestingly, MVs often have a more symmetrical distribution of lipids in their membranes, including exposing PS and other lipids normally sequestered only to the inner leaflet on their outer surface [53,54]. Ca^{2+} inhibits flippase activity while promoting scramblase activity, resulting in an increase in PS in the PM external leaflet [45,55,56].

In humans and mice, phospholipid scrambling can be accomplished by the Ca^{2+-} dependent TMEM16F protein, a Ca^{2+}-gated Cl^- channel that also functions as a Ca^{2+-} dependent scramblase [40,57]. Required for PS exposure in the coagulation cascade, a mutation in TMEM16F in platelets leads to a clotting disorder called Scott Syndrome in humans, caused by a defect in ectosome release [51,58]. Similarly, in neutrophils treated with the pore forming agent LLO derived from *Listeria monocytogenes*, TMEM16F was required for proper membrane repair, PS exposure, and ectosome release through which damaged lipids and toxins were removed [16]. Addition of the Ca^{2+}chelator ethylene glycol tetra-acetic acid to LLO treated cells blocked membrane repair, indicating Ca^{2+} controls the mechanism of EV release [16]. Whether scramblases play a role in MV biogenesis in other cell types is unknown.

1.3 The Role of Microdomains in Cargo Sorting and MV Biogenesis

Although alterations in EV membrane transverse lipid organization has an established role in MV biogenesis, recent studies have indicated that lateral distribution of lipids and proteins within each leaflet may also have a unique purpose in MV biology. Short-lived or stable groupings of particular macromolecules within a lateral plane, such as is seen in lipid rafts which are comprised of sphingolipids, cholesterol, and GPI anchored proteins or regions that are enriched in tetraspanins or caveolae, may give rise to unique populations of EVs. In red blood cells, a minimum of three separate microdomains have been characterized: cholesterol dense, GM1 dense, and sphingomyelin dense [41]. Each of these domains may play a role in inducing membrane curvature, acting as a platform for EV budding or working to repair the membrane after budding occurs. In platelets, cholesterol rich domains are likely regions of EV budding during platelet activation, while regions dense in PIP_2 are stable, and artificial increases in PIP_2 density create vesiculation-resistant areas within the membrane[41]. However, in other cell types concentrated PIP_2 might induce membrane curvature [59].

Based on this information, it is hypothesized that, within a single cell, proteins and lipids could localize to a specific microdomain within the PM distinct from surrounding regions. Their inclusion in that microdomain would allow them to be released in an EV derived from that small region controlled by certain proteins and triggers. Simultaneously, another microdomain could exist in the same cell characterized by different lipids and cargo, and its biogenesis controlled by a unique mechanism. This could allow individual launch sites for vesicle subpopulations concurrently from the same cell[41]. Further research is needed to understand the role of lipid microdomains in MV biogenesis.

1.4 Cilia Structure and Ciliary Derived EVs

Cilia in many organisms are a known site of microvesicle release [60]. Cilia are formed via a conserved mechanism seen in most eukaryotes called intraflagellar transport (IFT). There are three sections of the cilia – the proximal region, the middle region, and the distal region. The proximal region contains a basal body followed immediately by the transition zone. The transition zone plays an important role in regulating the movement of proteins, lipids, and other molecules in and out of the cilia. It acts as a selective gate, allowing passage of only specific molecules[61]. As a result, cilia are able to maintain tightly controlled levels of $Ca^{2+}$and other second messengers without affecting the remainder of the cell, and completely exclude the entrance of certain molecules, such as PIP_2, from entering the cilia [10,61,62]. The middle segment of the cilia is made up of microtubule doublets and in *C. elegans* is built by kinesin-2 motors OSM-3 and Kinesin-II, while the distal segment is composed of microtubule singlets and is built solely by OSM-3 [63].

1.4.1 *C. elegans* Ciliated Sensory Neurons Release EV

Caenorhabditis elegans, a nematode which naturally resides in soil, is a meticulously characterized model for studying physiological and pathological processes. Its transparent body lends itself easily to fluorescent imaging experiments, while its roughly three-day life cycle, large brood sizes, and bacterial diet allow for easy maintenance. Their ability of hermaphrodites to reproduce through self-fertilization or through mating with and males allows for simple genetic manipulation. Roughly 60-80% of human genes have a *C. elegans* homolog, and many disease pathways are conserved. Its 959 cells, including 302 neurons, have been individually characterized and their unique functionalities studied[64].

Ciliated sensory neurons in *C. elegans* are neurons that extend from cell bodies in the head and tail and terminate in short primary cilia at the dendritic tip. Of the 112 ciliated sensory neurons, some have ciliated dendrites that extend through the cuticle and access the external environment [63]. These neurons include the inner labial type 2 neurons, and cephalic male (CEM) neurons found in the head, and hook B type (HOB) and bilateral ray B type (RnB) neurons located in the tail. Surrounding the ciliary base is a glial sheath cell, which is connected to the cuticle via a socket cell. EVs bud from the sensory neuron cilia and then are either released into the external environment or taken up by the surrounding sheath and socket glial cells. Additionally, a lumen exists between the glia and the neuronal cilia, and this luminal space is a site of EV storage [65] **(Figure 3)**.

C. elegans grow and maintain their cilia via IFT with anterograde and retrograde motors using machinery that is similarly conserved among other species including *Chlamydomonas* algae and vertebrates. Anterograde motors consist of the heterotrimeric kinesin-2 which contains two motor subunits, KLP-20 and KLP-11, with an accessory subunit called KAP1 and a homodimeric kinesin 2, with each subunit called OSM-3[66]. Retrograde transport is accomplished by IFT dynein motors which include multiple subunits, including a motor subunit CHE-3 and light intermediate chain XBX-1, which are commonly used as ciliary markers in *C. elegans*[66].

PKD-2 and LOV-1, homologs of mammalian polycystins PKD1 and PKD2, are found only in the 21 male specific neurons, localize specifically to the cilia, and are packaged into EVs released from the male and hermaphrodite head and male tail. Ciliary derived vesicles in *C. elegans* have been determined to be microvesicles, since MVBs are not observed in the cilia and proteins required for MVB formation, including the signal transducing adaptor protein STAM-1, MVB-12 which is a subunit of ESCRT-1, and ALX-1 which is necessary for late endosome formation, were not required for release of PKD-2 containing EVs [65].

According to current models, MVs bud from the ciliary tip and base in *C. elegans* ciliated sensory neurons in response to mechanical stimulation among other stimuli[67,68]. Distal segment shedding of PKD-2::GFP containing EVs requires myristolated coiled-coil protein CIL-7 enrichment in the tip [65,67,69]. Interestingly, CIL-7 and PKD-2 tend to occupy different subpopulations of EVs although they are released from the same regions, indicating a specialized sorting mechanism **(Figure 4)**[67]. Mutations in *cil-7* or *klp-6* cause EVs released from the periciliary membrane compartment (PCMC) of the ciliary base to be aberrantly stored in the lumen of the sheath cell surrounding the PCMC [65,69,70] .

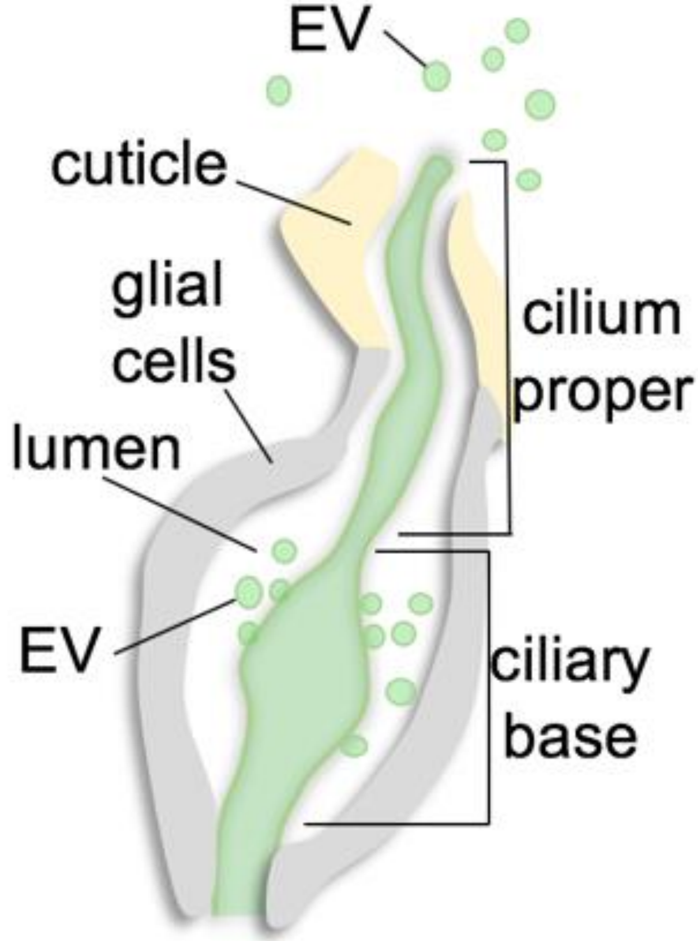

Figure 3: The structure of *C. elegans* ciliated sensory neurons. Cilia protrude through the cuticle to access the environment. EVs bud from the ciliary base and are stored in the lumen until stimulation induces release into the environment. EVs are also released from the distal ciliary segment.

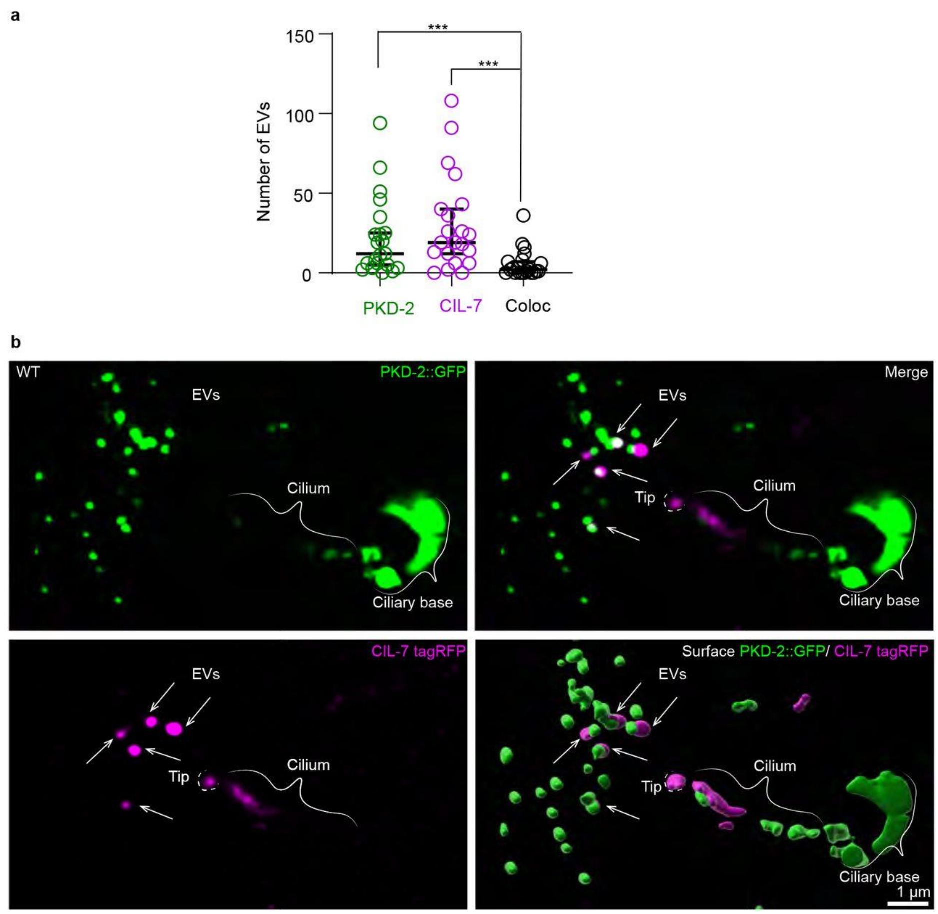

Figure 4: EV cargoes CIL-7 and PKD-2 occupy two subpopulations of EVs, rarely colocalizing. (A) The majority of EVs released fell into one of two EV subpopulations: PKD-2 or CIL-7 containing EVs. A smaller minority of EVs were colocalized. (B) Images of PKD-2::GFP and CIL-7::tagRFP EV release from amphid neurons. Figure adapted from Wang, et al., 2021.

Although CIL-7 and KLP-6 are required for EV shedding, no published research has described a biogenesis mechanism for MV budding from ciliated neurons. Further, it is unclear if all MVs bud from the ciliary base and tip or if they can also form from the middle segment of the cilia such as in *Chlamydomonas*. Further research is required to elucidate the mechanism and pinpoint the location of EV biogenesis from the ciliated sensory neurons in *C. elegans.*

1.5 A Powerful *C. elegans* Model for Studying EV Biogenesis

We have developed a *C. elegans* EV biogenesis model within the Tanis lab, providing powerful tools to shed light on these areas of research. The Tanis lab discovered that calcium homeostasis modulator 1 (CLHM-1), an ion channel that is expressed within the male ciliated sensory neurons and localizes to the cilia, is released in EVs [71]. Remarkably, when fluorescently labelled CLHM-1::tdTomato was expressed with fluorescently labelled PKD-2::GFP in the same transgenic worm, dual-colored fluorescence was seen in a significantly lower percentage of total EVs when compared to a CLHM-1::tdtomato; CLHM-1::GFP control **(Figure 5)**[71].

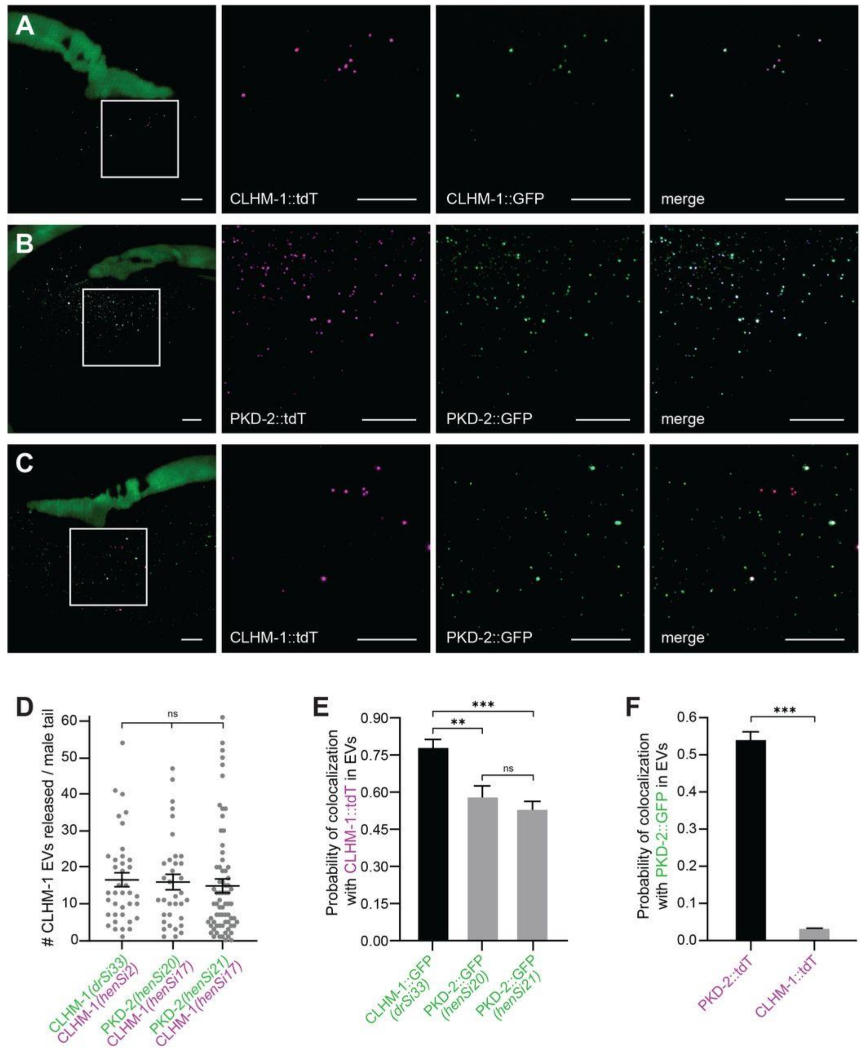

Figure 5: EV cargo CLHM-1 and PKD-2 occupy two separate subpopulations of EVs. (A) Animals expressing both CLHM-1::GFP and CLHM-1::tdTomato released mostly colocalized EVs. (B) Animals expressing both PKD-2::GFP and PKD-2::tdTomato released mostly colocalized EVs. (C) Animals expressing both PKD-2::GFP and CLHM-1::tdTomato released majority single-fluorophore tagged EVs. (D) CLHM-1 tagged EV release is not affected by the presence of CLHM-1::GFP (drsi33) transgene or the presence of PKD-2::GFP (hensi20) or PKD-2::GFP (hensi21). (E) The prevalence of colocalized EVs released from CLHM-1::GFP; CLHM-1::tdTomato background animals is greater than when compared to either PKD-2::GFP(hensi20); CLHM-1::tdTomato or PKD-2::GFP(hensi21); CLHM-1::tdTomato. Figure adapted from Clupper et al., 2021.

The overarching goal of this research was to characterize the mechanism(s) underlying the release of specific EV subpoluations. First, I sought to characterize the localization of CLHM-1 in ciliary subcompartments and in relationship to other ciliary proteins known to be released as EV cargo or involved in EV shedding. Secondly, I investigated the role of interflagellar transport proteins on CLHM-1, and PKD-2 ciliary and EV colocalization. Finally, I explored the possible role of two scramblase proteins in CLHM-1 EV biogenesis.

Chapter 2

MATERIALS AND METHODS

2.1 Culturing *C. elegans*

C. elegans were cultured and maintained according to the instructions previously described in Brenner 1974. Worms were grown on NGM media and incubated at 20º C with OP50 *Escherichia coli* as their food source.

2.2 NGM Media

To prepare NGM Media for *C. elegans* culture, 34 g agar, 6 g NaCL, and 5 g of peptone were added to 2 liters of DI water in a 6 liter bottle. The mixture was autoclaved on 40-minute cycle. After being cooled for one hour at 70 C, 2 mL of 4 mg/mL cholesterol in ethanol, 2 mL of 2 M $CaCl_2$, 2 mL of 1 M $MgSO_4$, and 50 mL of 1 M KPO4 were stirred into the solution for 15 minutes at 55º C. A DWK Life Sciences Wheaton OmniSpense Elite Peristaltic Pump (Cat #13687446) was employed for dispensing the media into plates. 3.5 mL of media was dispensed into the 30 mm plates, 10 mL of media into the 60 mm plates, and 25 mL of media into the 100 mm plates. Plates dried at room temperature overnight and were seeded with OP50 *E. coli*.

2.3 Feeding and Maintaining *C. elegans*

OP50 was cultured in liquid LB broth using aseptic technique and incubated at 37º C for approximately 18 hours. A repeating pipette was used to seed plates with the following amounts of inoculated broth: 100 µl of broth on 30 mm plates, 250 µl of broth on 60 mm plates and 500 µl of broth on 100 mm plates. After plates had dried fully, in 1-3 days, at room temperature, plates were inverted for storage at room temperature to be used immediately or at 4º C for long term storage.

Maintenance of animals was conducted using a platinum wire pick to move three L4 animals to a new plates approximately every 3 days. These plates were stored at 20º C for three days and their progeny were maintained in the same way to new, seeded plates. Animals not actively needed for experimentation were stored at 15º C and maintained once a week. To revive a strain for experiments a chunk of media from a starved plate kept at 15º C was aseptically cut out and places onto a new plate. Animals were incubated at 20º C and L4 progeny were transferred to new plates for maintenance at least once before experimentation was conducted.

2.4 Strains of *C. elegans*

Strains utilized in the research included in this thesis are detailed in Table 1. Strains with names that include UDE were generated in the Tanis Laboratory at the University of Delaware.

Table 1 ***C. elegans*** **strains**

Strain	Description
UDE76	henSi2 [Gclhm-1::tdTomato::let858 3'UTR] I ; drsI33[clhm-1p::clhm-1::gfp] II ; him-5(e1490) V
UDE165	henSi17 [Pklp-6::clhm-1::tdTomato::let858 3'UTR] I; henSi20 [Ppkd-2::pkd-2::GFP::let858 3' UTR] IV; him-5 (e1490) V
UDE175	henSi17 [Pklp-6::clhm-1::tdTomato::let858 3'UTR] I; henSi21 [Ppkd-2::pkd-2::GFP::let858 3' UTR] ; him-5 (e1490) V
UDE151	henSi17 [Pklp-6::clhm-1::tdTomato::let858 3'UTR] I; mks-5 (ok3582) II; henSi20 [Ppkd-2::pkd-2::GFP::let858 3' UTR] IV; him-5 (e1490) V
UDE159	henSi2 [Gclhm-1::tdTomato::let858 3'UTR] I; mks-5 (ok3582) II; drsI33[clhm-1p::clhm-1::gfp] IV; him-5 (e1490) V
UDE106	henSi17 [Pklp-6::clhm-1::tdTomato::let858 3'UTR] I; clhm-1 (tm4071) II; henSi20 [Ppkd-2::pkd-2::GFP::let858 3' UTR] IV; him-5 (e1490) V
UDE27	drsi33[clhm-1p::clhm-1::gfp] IV; him-5 (e1490) V
UDE130	henSi17 [Pklp-6::clhm-1::tdTomato::let858 3'UTR] I ; him-5 (e1490) V; myIs23[Pcil-7::gCIL-7GFP_3'UTR + ccRFP] X
UDE119	che-3(cas443{gfp::che-3])I; hensi2[Gclhm-1::tdtomato::let858 3' UTR; him-5 (e1490)V]
UDE127	anoh-1(TM4762)III; drsi33 [clhm-1p::clhm-1::gfp] IV; him-5 (e1490)V
UDE135	anoh-1 (TM4762) III; henSi20[Gpkd-2::GFP::let858 3'UTR] IV; pkd-2 (sy606) IV; him-5 (e1490) V
PHX2610	anoh-1::gfp (syb2610)
UDE184	henSi17 [Pklp-6::clhm-1::tdTomato::let858 3'UTR] I; osm-3 (mn391) IV; henSi21 [Ppkd-2::pkd-2::GFP::let858 3' UTR] ; him-5 (e1490) V
UDE195	henSi17 [Pklp-6::clhm-1::tdTomato::let858 3'UTR] I; klp-11 (tm324) IV; henSi21[Ppkd-2::pkd-2::GFP::let858 3' UTR]; him-5 (e1490) V
UDE198	henSi17 [Pklp-6::clhm-1::tdTomato::let858 3'UTR] I; osm-3 (p802) IV; henSi21[Ppkd-2::pkd-2::GFP::let858 3' UTR]; him-5 (e1490) V
PHX2611	anoh-2::gfp (syb2611)
UDE121	anoh-1(tm4762); him-5(e1490) V

2.5 Preparing genetic crosses

In order to generate fluorescently labelled strains in IFT and the scramblase mutant background, the following method was used as the guideline. Transgenic strains with fluorescently labelled EV marker proteins in the *him-5* (high incidence of males) background were mated with worms with the desired mutations also with a *him-5* mutation in the background. Six L4 F1 animals were plated individually onto 6 separate plates. From each of those plates, six F2 L4 progeny from each plate were staged in isolation for a total of 36 separate F2 plates. Each of those plates were screened for the fluorescent marker. Lines that were confirmed to be homozygous for the fluorescent transgene were then genotyped for the desired mutation(s) using primers. Multiple F2 adult progeny from each fluorescently positive plate were submerged 10 µl of lysis buffer containing the following ingredients: 50 mM KCl, 10 mM Tris (pH 8.3), 2.5 mM MgCl2, 0.45% NP-40, 0.45% Tween-20, and 0.01% Gelatin and proteinase K. Worms in the lysis solution were cooled at -80º C for a minimum of 10 minutes before lysis. Animals were lysed at 60º C for 1 hour and then 95º C for 15 minutes. PCR was then performed on the DNA from the lysed animal using 2x Green GoTaq Master Mix and primers designed to detect the mutation of interest.

2.6 Airyscan confocal microscopy

Worms used to collect images of cilia or EV release were prepared in the following way: between 20-30 L4 stage males were separated onto a new seeded plate in the presence of at least 10 adult hermaphrodites approximately 24 hours before images were obtained. At the time of imaging, worms were picked onto 3% agar pads on slides that were roughly the size of coverslips. Approximately 7-10 worms were paralyzed on each slide in 10 µL of 10mM levamisole and covered with a cover slip before imaging. Z stacks were obtained using the Zeiss LSM880 63x oil objective with Airyscan GaAsP-PMT area detector. Images were processed using standard Airycsan processing settings and were analyzed further using Volocity (PerkinElmer).

Volume quantitation of ciliary colocalization and fluorescence intensity were measured in three-dimensions. To measure Manders Correlation Coefficients (M1 and M2), a ROI was drawn around each cilia proper and ciliary base, using the transition zone as the demarcation between the two regions. A high value Manders coefficient indicates a large overlap of both types of fluorescently tagged molecules within a particular region, while the relationship between M1 and M2 indicates pixel spread.

2.7 Statistical analysis

The Anderson-Darling normality test was utilized to determine the normality of each dataset. When comparing two data sets, normal data was further analyzed using Student's t test while the Mann-Whitney U test was conducted on data that did not follow a normal distribution. A one-way ANOVA or Kruskal-Wallis test with multiple comparisons was done to compare three or more data sets. All statistical analyses and graphing were conducted with GraphPad Prism 9.

2.8 Ionomycin assays

Between 20-30 L4 stage virgin males were separated onto a new seeded plate in the approximately 24 hours before images were obtained. Worms were staged on slides containing circular 3% agar pads. Approximately 7 worms were paralyzed with either 6 µL of levamisole or 3 µL of levamisole and 3 µL of 1 µM ionomycin. Within 30 minutes of mounting, Z stacks of released EVs were obtained using the Zeiss LSM 880 63x oil objective with GaAsP-PMT area detector. Images were processed using standard Airycsan processing settings.

Chapter 3

RESULTS

3.1 EV cargo CLHM-1 has a unique localization pattern within the cilia of ciliated sensory neurons

Current hypotheses of EV biogenesis mechanisms in *C. elegans* suggest that EVs bud from either the ciliary base or the distal segment[67]. After determining CLHM-1 was expressed within the ciliated sensory neurons, further investigation was needed to determine the regions where the protein could be found as an indicator of potential EV budding location. To determine where CLHM-1 localized within the cilia, I imaged the RnB tail neurons in transgenic strains which co-expressed CLHM-1::tdTomato with either CIL-7::GFP or CHE-3::GFP. CIL-7 is required for PKD-2::GFP containing EV release from the ciliary tip, and as such is known to localize to the distal segment of the cilia as well as the PCMC[67,69]. CIL-7 is also observed to be excluded from the transition zone, while present in the middle segment and the PCMC, demarcating the transition zone with its absence[69]. CHE-3::GFP, an IFT dynein motor subunit and a characterized ciliary marker not released in EVs, fills out the distal segment, and is sparsely localized in the middle segment [72]. Visual analysis of images showed that CLHM-1 was excluded from the distal segment of the cilia and failed to colocalize with either CIL-7 or CHE-3 in that region **(Figure 6A)**. CLHM-1 co-localizes with CIL-7 in the middle segment, is excluded from the transition zone, and is observed in the PCMC **(Figure 6A)**.

To quantify the colocalization of CLHM-1 with these markers, I analyzed these images using Volocity to calculate Manders correlation coefficients. M1 describes the incidence of GFP pixels that also overlap tdTomato pixels, while M2 represents the incidence of tdTomato pixels that also overlap GFP pixels. Compared to the overlap of CLHM-1::GFP; CLHM-1::tdTomato in the control animals, there was a significantly lower percent colocalization of CLHM-1 with both CIL-7 and CHE-3, indicating that these proteins occupy distinct areas within the cilia (**Figure 6B**). The low M2 value for animals expressing CHE-3::GFP; CLHM-1::tdTomato suggests that the majority of CLHM-1::tdTomato is localized away from distally localized CHE-3::GFP, as less than 20% of red pixels also colocalize with green pixels (**Figure 6C**).

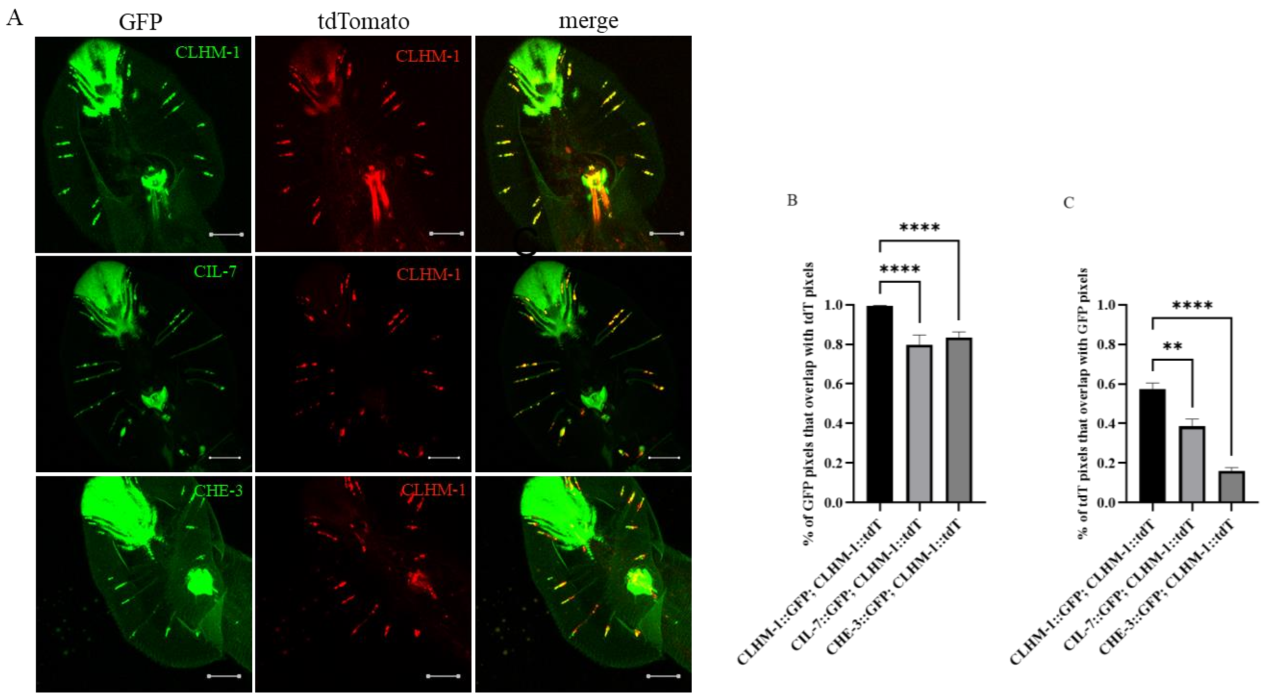

Figure 6: CLHM-1 localizes to the ciliary middle segment and PCMC but is excluded from the distal segment. (A) CLHM-1::tdT does not colocalize with either CIL-7::GFP or CHE-3::GFP in the distal segment of the cilia. CLHM-1 colocalizes with CIL-7 in the middle segment and the PCMC while being excluded from the transition zone. (B) Manders coefficient 1 (M1) which represents the percentage of GFP pixels that overlap with tdT pixels in significantly decreased in CIL-7::GFP; CLHM-1::tdT animals and in CHE-3::GFP; CLHM-1::tdT animals compared to CLHM-1::GFP; CLHM-1::tdT worms. (C) Manders coefficient 2 (M2) which represents the percentage of tdT pixels that overlap with GFP pixels is significantly decreased in CIL-7::GFP; CLHM-1::tdT animals and in CHE-3::GFP; CLHM-1::tdT animals compared to CLHM-1::GFP; CLHM-1::tdT animals.

3.2 EV cargoes PKD-2 and CLHM-2 exhibit incomplete colocalization within the cilia

Upon discovering that CLHM-1 and PKD-2 were packaged into unique EV subpopulations, we sought to determine if spatial organization within the cilia might play a role in protein sorting into EVs. We hypothesized that regions containing only PKD-2 or CLHM-1 might the be the origin of single fluorophore labelled EVs while colocalized EVs might bud off from colocalized regions. I imaged cilia of RnB neurons in transgenic animals labelled with CLHM-1::tdTomato and PKD-2::GFP and compared fluorescent protein colocalization and intensity to control transgenic animals labeled with CLHM-1::tdTomato and CLHM-1::GFP (**Figure 7A**).

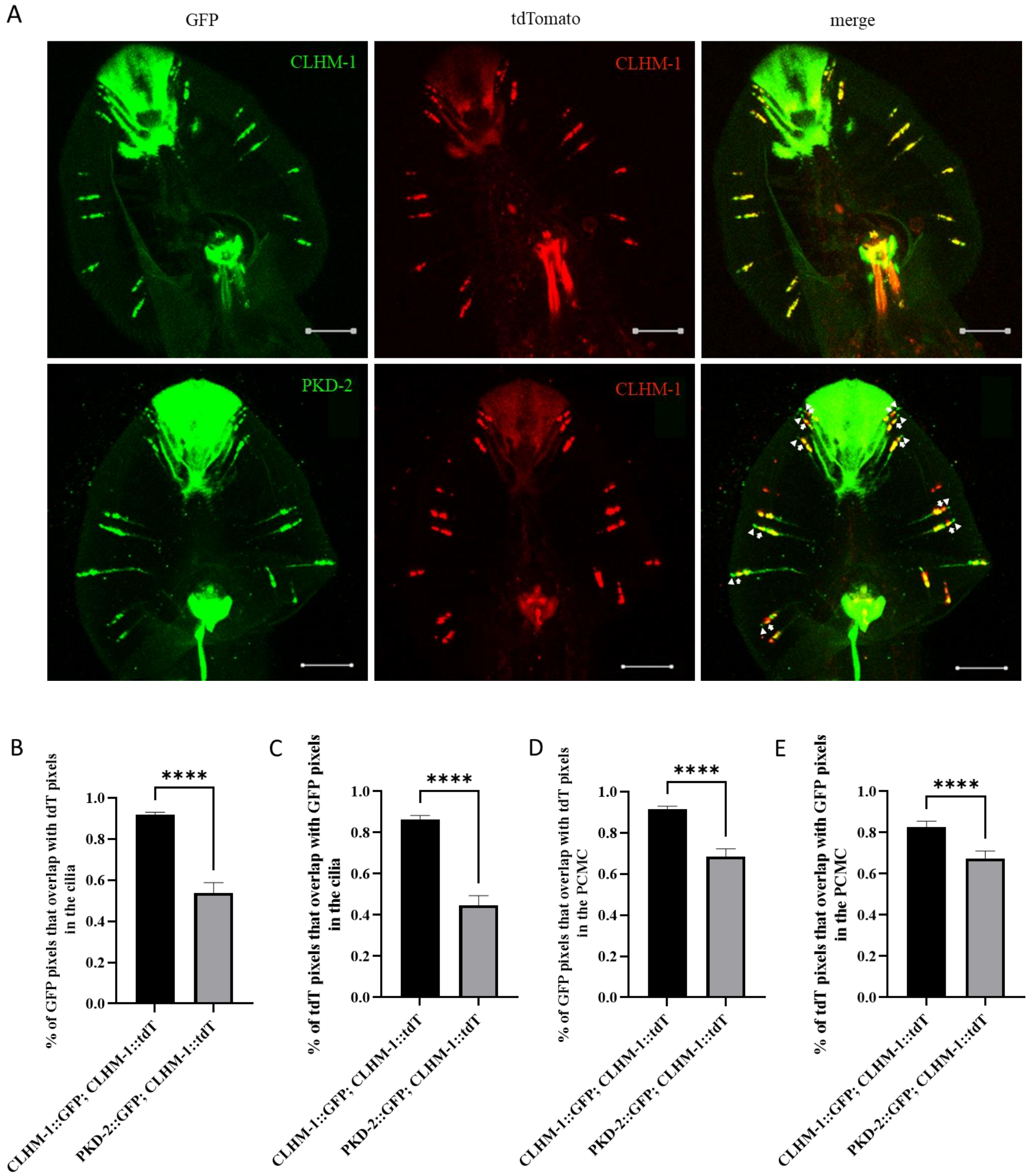

Figure 7: PKD-2, but not CLHM-1, localizes to the ciliary tip while partial colocalization is seen in the middle segment and PCMC. (A) CLHM-1 is excluded from the distal tip where PKD-2::GFP is seen. Arrowheads mark distal tip and arrows mark the middle segment. (B-E) PKD-2::GFP and CLHM-1::tdT displayed decreased colocalization compared to CLHM-1::tdT and CLHM-1::GFP in the control animals.

PKD-2 and CLHM-1 both localized to the middle segment and cilia proper while being excluded from the transition zone. However, only PKD-2 was seen in the distal segment of most cilia (**Figure 7A**). I then performed a three-dimensional quantification of the colocalization between CLHM-1::tdTomato with CLHM-1::GFP or PKD-2::GFP. A decrease in M1, which is the percentage of GFP pixels colocalized with tdTomato pixels was seen in the CLHM-1::tdTomato; PKD-2::GFP animals compared with the control in both the cilia proper and PCMC regions (**Figure 7B,D**). This supports our visual observations and indicates that a region in the distal portion of the cilia contained GFP only, while portions PCMC were also consistently only green. Additionally, I investigated the percentage of tdTomato pixels that were overlapping with GFP pixels using Manders 2 (M2) coefficient. Again, the coefficient was lower in the cilia and PCMC of CLHM-1::tdTomato; PKD-2::GFP animals compared to the control indicating less colocalization (**Figure 7C,E**). These data were also consistent with our visual observations of isolated regions of tdTomato in the middle segment and in the PCMC.

Two-dimensional fluorescence intensity analyses of ciliary image projections from PCMC (denoted by base in the projection) through the cilia proper were conducted to provide additional information about the localization pattern of PKD-2 and CLHM-1. These intensity projections showed that CLHM-1::tdTomato was excluded from the ciliary tip while PKD-2::GFP consistently localized to the distal segment (**Figure 8A**). Based on these findings, a model for single fluorophore and colocalized EV release is suggested with PKD-2::GFP EVs being released from the distal segment, CLHM-1::tdTomato EVs budding from the middle segment, while dual-labelled EVs originate from the ciliary base (**Figure 8B**).

A

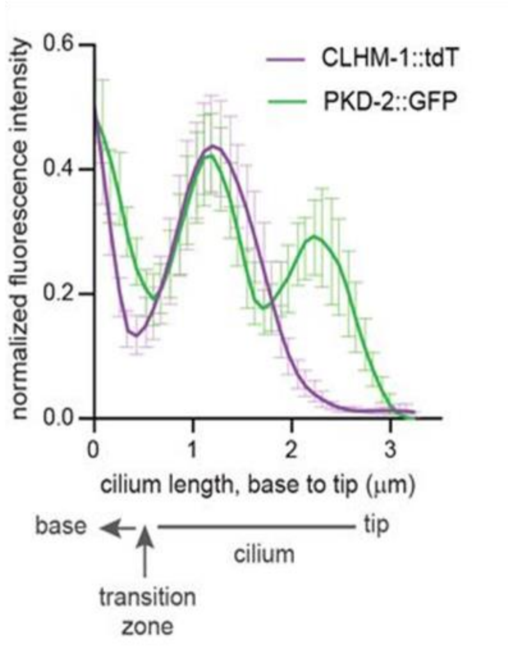

B

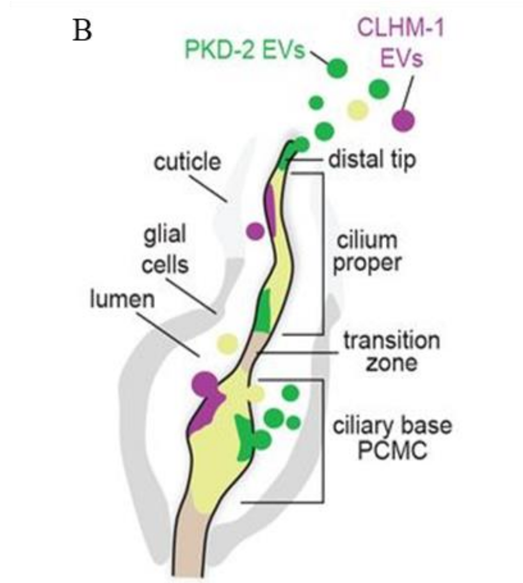

Figure 8: Ciliary localization patterns are distinct for PKD-2 and CLHM-1. (A) Fluorescent intensity projections for CLHM-1::tdT and PKD-2::GFP. PKD-2::GFP intensity spikes in the PCMC, middle segment and distal tip. CLHM-1::tdT peaks in the PCMC and middle segment. (B) A model of EV release for CLHM-1 and PKD-2 subpopulations. PKD-2 EVs bud from the ciliary tip and base from discrete PKD-2 containing regions, while CLHM-1 EVs originate in the middle segment of the cilium proper and base from regions that contain concentrated amounts of CLHM-1. Colocalized EVs can originate from colocalized areas. Figure adapted from Clupper et al, 2021.

3.3 KLP-11 and OSM-3 regulate abundance of CLHM-1 within the cilia and in EVs

IFT regulates the abundance and localization of ciliary proteins along with assembling and regulating the dynamic ultrastructure of the ciliary regions. Anterograde transport in *C. elegans* ciliated sensory neurons is conducted by the heterotrimeric kinesin-2 made up of KLP-11, KLP20 and KAP-1 and the homodimeric kinesin-2 OSM-3. We hypothesized that trafficking of the EV cargo proteins CLHM-1 and PKD-2 from the PCMC to the middle and distal segments was accomplished by these motors and that mutations in the complex subunits might cause changes in cargo ciliary localization and release in EVs.

Another graduate student in the lab, Michael Clupper, examined the effects of these mutations on EV release. He found that *klp-11(tm324)*, *osm-3(mn391)*, and *osm-3(p802)* animals did not release an increased amount of PKD-2 containing EVs but did release a higher quantity of CLHM-1 containing EVs (**Figure 9A,B**). Additionally, both *osm-3* mutations increased the incidence of CLHM-1::tdTomato EVs also containing PKD-2::GFP (**Figure 9C**).

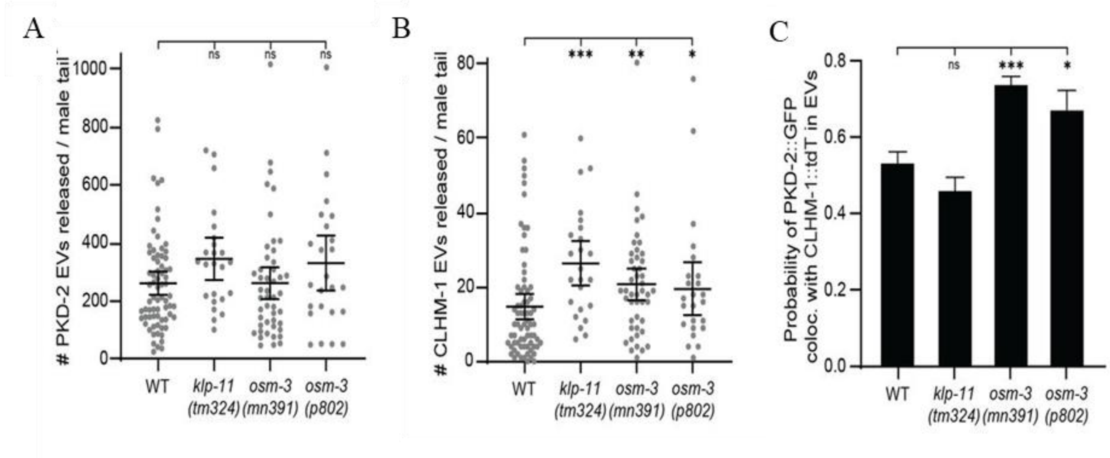

Figure 9: KLP-11 and OSM-3 regulate abundance of CLHM-1 containing EV (A) *klp-11* and *osm-3* had no significant effect on PKD-2::GFP containing EV abundance. (B) CLHM-1 containing EVs are released more frequently in *klp-11* and *osm-3* animals. (C) *osm-3* causes an increase in the incidence of PKD-2::GFP containing EVs that also contain CLHM-1::tdT. Figure adapted from Clupper et al, 2021.

I then investigated the impact of these kinesin-2 mutants on the colocalization of CLHM-1::tdTomato and PKD-2::GFP in the cilium proper and PCMC of the biliary base. Loss of *klp-11* caused a significantly increased percentage of GFP pixels colocalized with tdTomato pixels in the cilia proper, while a significantly decreased percentage of tdTomato pixels overlapped in the same region (**Figure 10A-B**). The same trend was seen in the PCMC (**Figure 10C-D**). No significant change was seen in the *osm-3* backgrounds.

I found that all three mutations caused a decrease in CLHM-1::tdTomato average intensity in the PCMC, but no significant changes in CLHM-1 intensity were observed in the cilia (**Figure 11A-B).** A decrease in CLHM-1::tdTomato intensity in the PCMC correlated with the overall increase in CLHM-1 containing EV release (**Figure 9B**). The distribution of PKD-2 and CLHM-1::GFP within the cilia and PCMC in *klp-11* and *osm-3* were similar to WT, with intensity peaking for PKD-2 GFP in base, middle segment and tip, while CLHM-1::tdTomato was seen in the same regions except being largely excluded from the ciliary tip [71] .

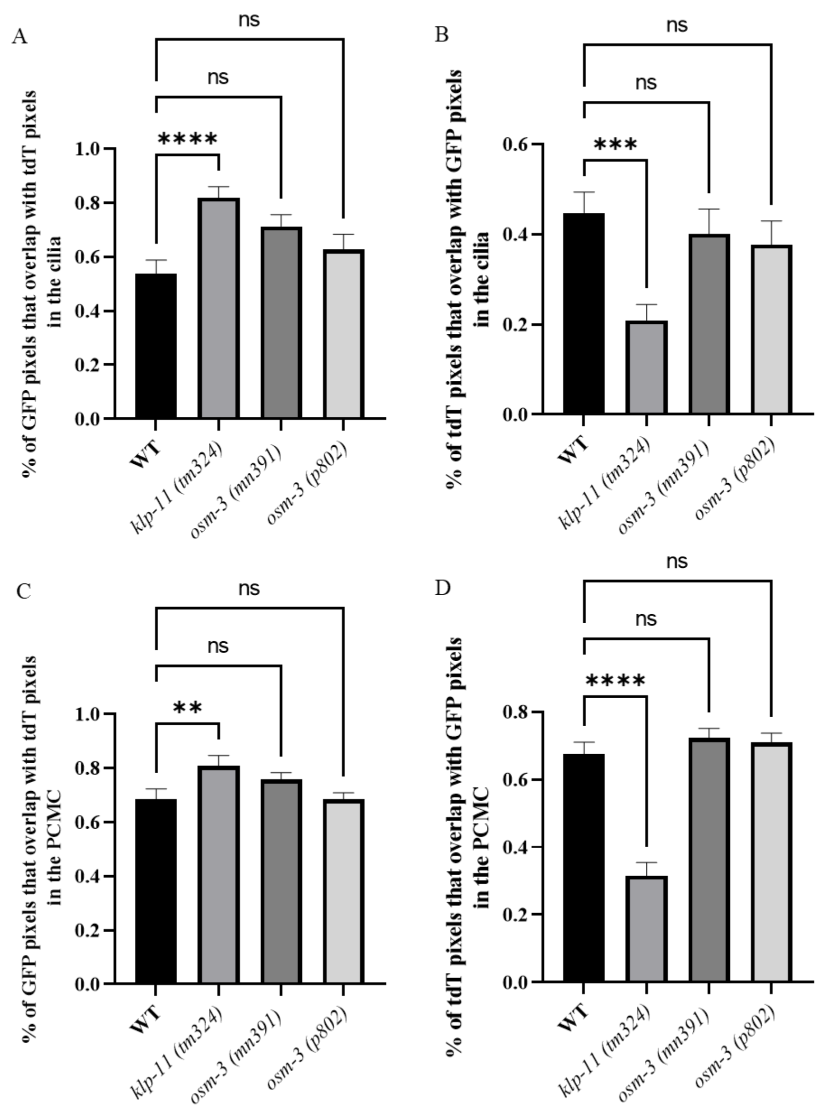

Figure 10: Loss of *klp-11* causes a change in colocalization of PKD-2::GFP and CLHM-1::tdT in the cilia and PCMC. (A,C) An increased percentage of GFP pixels overlapped with tdT pixels in the cilia when compared to WT in k*lp-11* but not in *osm-11*. (B,D) A decreased percentage of tdT pixels overlapped with GFP pixels in the cilia when compared to WT in *klp-11* but not in *osm-3.*

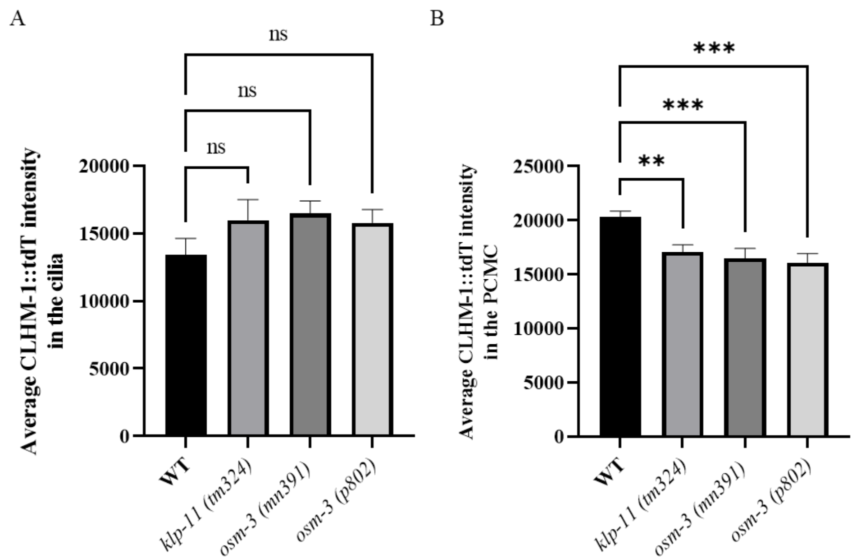

Figure 11: CLHM-1 abundance in the cilia proper is unaffected by anterograde motor mutations, but is decreased in the PCMC. (A) No significant difference in average intensity of CLHM-1::tdT in the cilia was observed in *klp-11* or *osm-3* animals. (B) IFT anterograde motor subunits KLP-11 and OSM-3 play a role in regulating CLHM- 1 localization within the PCMC demonstrated by a significant decrease in CLHM-1::tdT intensity.

3.4 Anterograde IFT is required for proper localization and EV release of PKD-2, but not CLHM-1

The homodimeric kinesin OSM-3 motor and the heterotrimeric kinesin made up of KLP-11, KLP20 and KAP-1 display partial redundancy in their role in anterograde IFT transport [73–76]. We asked what affect fully disabling anterograde transport might have on EV release and EV cargo protein localization within the cilia. We created an *klp-11(tm324); osm-3(mn391)* double mutant that expressed both CLHM-1::tdTomato and PKD-2:GFP and measured EV release. PKD-2::GFP release was almost completely obstructed, while there was no significant decrease in CLHM-1::tdTomato EV release[71]. In addition, a significantly decreased percentage of PKD-2 containing EVs colocalized with CLHM-1 compared to WT [71] .

Interestingly, I found that the percentage of PKD-2::GFP that overlapped with CLHM-1::tdTomato in the PCMC greatly increased, while the percentage of CLHM-1::tdTomato that overlapped with PKD-2::GFP decreased significantly in *klp-11; osm-3* animals **(Figure 12A-B)**. The three dimensional average intensity analysis of CLHM-1::tdTomato within the cilia proper was unchanged, while it decreased in the PCMC, suggesting that CLHM-1 is moved into the cilia via an OSM-3 and KLP-11 independent mechanism (**Figure 13A-B**). Two dimensional intensity projections of PKD-2::GFP localization within the cilia and PCMC revealed a striking change compared to WT. In the RnB neurons of *klp-11; osm-3* animals, PKD-2 was almost entirely excluded from the ciliary tip (**Figure 13**C).

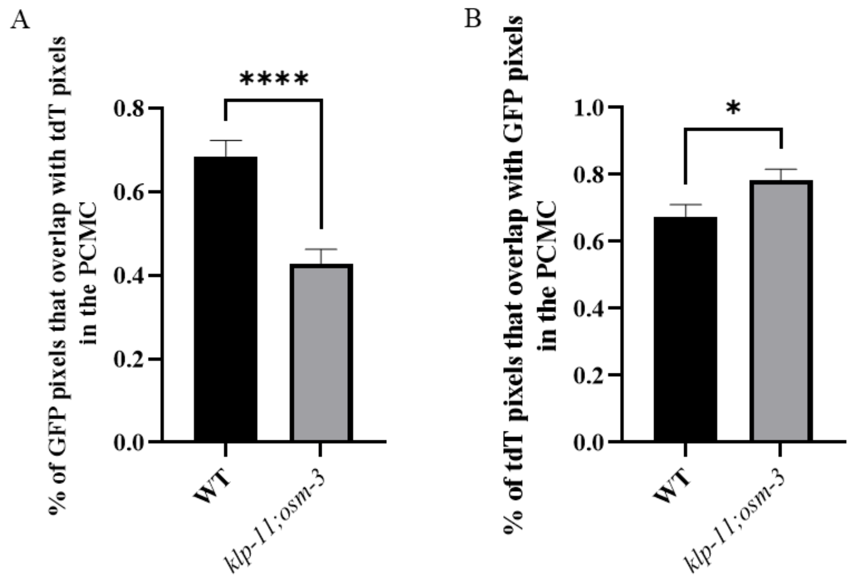

Figure 12: *klp-11; osm-3* double mutant animals exhibit changes in protein localization. (A) M1 was significantly increased in the PCMC of *klp-11; osm-3* animals. (B) M2 was significantly decreased in the PCMC of *klp-11; osm-3 animals.*

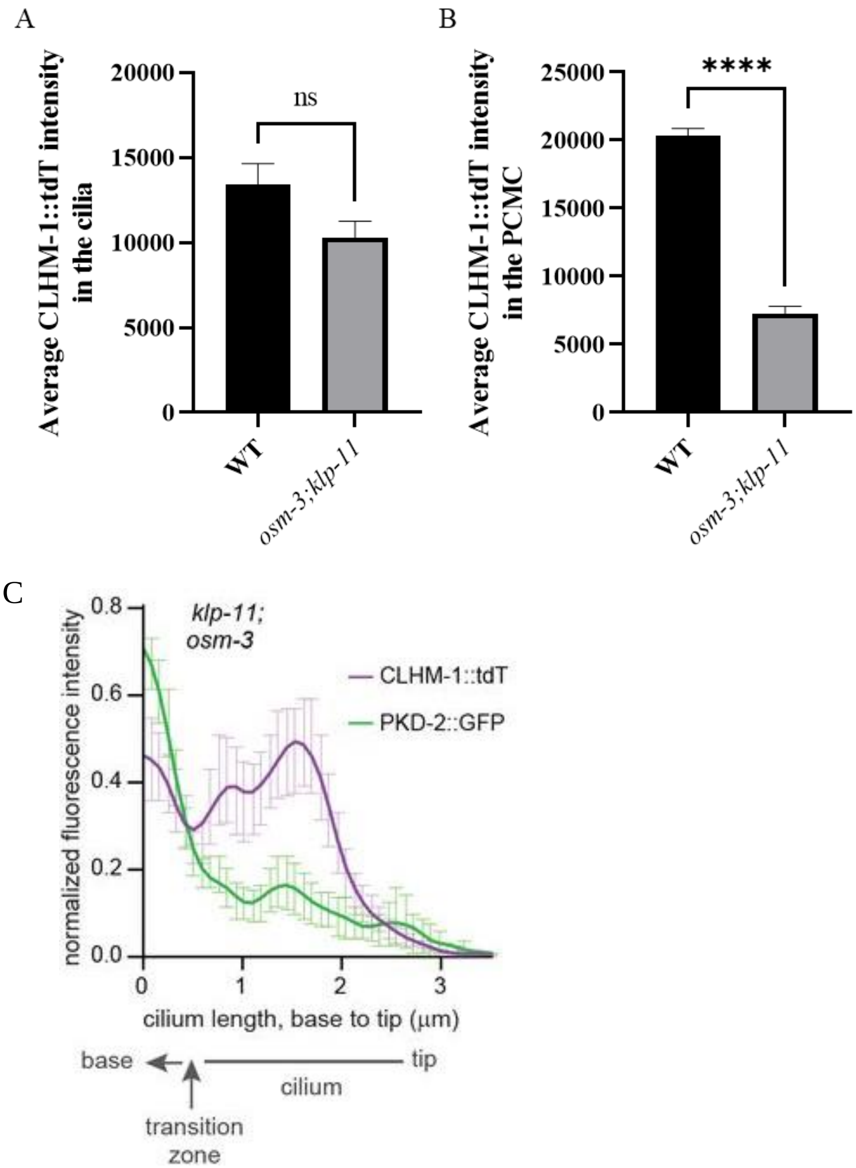

Figure 13: Normal abundance of CLHM-1 in the cilia proper does not require anterograde transport. (A) Average CLHM-1::tdT intensity in the cilia proper was not affected by mutations in KLP-11 and OSM-3 which disabled normal anterograde IFT. (B) Anterograde transport is required for normal abundance of CLHM-1 within the PCMC. C) *In klp-11; osm-3* animals, PKD-2 was almost entirely missing from the distal ciliary tip and tended to have a lower intensity in the middle segment when compared to wild-type.

3.5 Mutations in *mks-5* significantly alter ciliary structure and EV cargo colocalization

Alterations to the structure of the transition zone can lead to ciliary malformation along with aberrant protein and lipid localization within the cilia [77]. MecKel-Gruber Syndrome (MKS) homolog 5 (MKS-5) is a scaffolding protein critical to the formation and functionality of the transition zone in forming the periciliary membrane gate [61,77,78]. Mutations in *mks-5* result in atypical localization of signaling proteins and lipids within the cilia and increased IFT velocity[77]. I asked how these alterations in ciliary transport and compartmentalization might affect EV cargo localization in the cilia.

An *mks-5 (ok3582)* deletion mutant was crossed into a line expressing PKD-2::GFP and CLHM-1::tdTomato. My imaging revealed abnormalities in the 24-hour post L4 adult male tail, presenting as an irregular fan resembling the L4 male tail (**Figure 14A**). Additionally, in the *mks-5* mutant, truncated cilia indicating axoneme irregularities were observed (**Figure 14A**). Colocalization of PKD-2::GFP;CLHM-1::tdTomato was significantly greater in the *mks-5* mutant compared to wild type. Although the M2 analysis showed minimal differences in co-occurrence in the *mks-5* background, the M1 coefficient increased in both the PCMC and cilia compared with WT (**Figure 14B-E**). This increase in colocalization in the *mks-5* cilia and PCMC correlates with the increased colocalization of PKD-2::GFP and CLHM-1::tdTomato in the EVs released from these animals (M. Clupper, personal communication).

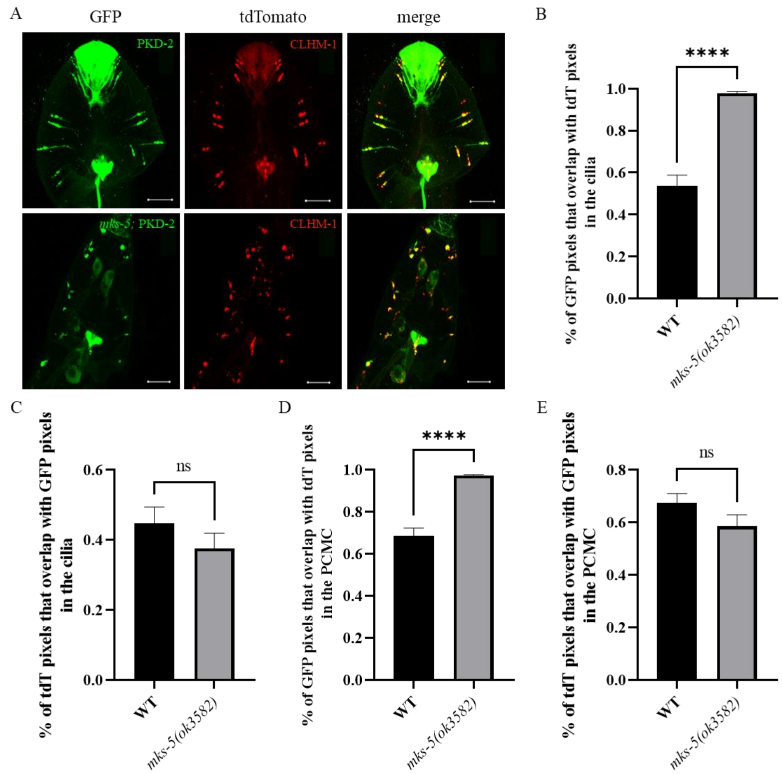

Figure 14: Cilia of *mks-5(ok3582)* animals are truncated and display abnormal CLHM-1 and PKD-2 colocalization patterns. (A) RnB neuron ciliary and tail morphology in WT and *mks-5* animals in adult 24-hour post L4 stage males. *mks-5* tail is atypical, with truncated cilia and a failure in tail retraction. (B) M1 coefficient representing percentage of GFP pixels colocalized with tdT pixels is significantly increased in the cilia of *mks-5* animals. (C) M2 coefficient which represents the percentage of tdT pixels which overlap with GFP pixels was not significantly increased in *mks-5*. (D) M1 coefficient was significantly increased in the PCMC of *mks-5* mutants. (E) M2 coefficient was not significantly altered in *mks-5* animals.

3.6 Scramblase ANOH-1 but not ANOH-2 is required for CLHM-1 containing EV release

In addition to seeking to learn what role ciliary protein organization plays in EV composition, I also sought to identify what role lipid changes might play in EV biogenesis. Evidence suggests that translocase-mediated PM lipid asymmetry alterations are a crucial step in EV biogenesis [79–82]. Because of this, a literature search was conducted to identify proteins with translocase capabilities that localize to the ciliated sensory neurons in *C. elegans.* The TMEM16 family, also called the Anoctamin family, includes multiple proteins which exhibit both Ca^{2+} channel and scramblase activity [57,83]. ANOH-1 and ANOH-2 are Ca^{2+} regulated anoctamin channels that are the closest homologs to human TMEM16F found in *C. elegans* [80,84,85]. ANOH-1 is required for PS exposure in necrotic but not apoptotic cells and has been hypothesized to play a role in promoting phagocytosis of cellular debris [80,84]. A since retracted paper indicated that ANOH-1 and ANOH-2 localized to the ciliated sensory neurons in *C. elegans*, specifically the amphid and phasmid neurons [85]. To determine if these proteins localized to the cilia of male sensory neurons, two strains were generated by CRISPR/Cas9 to express fluorescently labelled ANOH-1::GFP and ANOH-2::GFP at single copy. My preliminary images of the strains suggest that ANOH-1::GFP and ANOH-2::GFP localize to the cilia of sensory neurons in the hermaphrodite head (**Figure 15**). I then crossed ANOH-1::GFP with CLHM-1::tdTomato and the *him-5* mutation, which causes progeny to have a high incidence of males [86]. ANOH-1::GFP appeared to localize in the cilia of the male ciliated sensory neurons of the tail and was noticeably colocalized with CLHM-1::tdTomato in the cilia (**Figure 16**). Colocalization of ANOH-1 with CLHM-1::tdTomato alongside ANOH-1 and ANOH-2 expression in the ciliated sensory neurons supports a possible lipid translocase role within the cilia.

To determine if ANOH-1 impacts EV biogenesis, I crossed *anoh-1(tm4762);him-5(e1490)* with either CLHM-1::GFP or PKD-2::GFP. I imaged these animals alongside WT controls to determine the effect the *anoh-1* mutation might have on EV release. PKD-2::GFP EV release was not significantly decreased in the *anoh-1* background when compared to wildtype (**Figure 17**). Interestingly, worms expressing CLHM-1::GFP in the *anoh-1* mutant background released significantly fewer CLHM-1::GFP containing EVs (**Figure 17**). This indicates that ANOH-1 may play a role in the biogenesis of the CLHM-1 containing EV subpopulation exclusively.

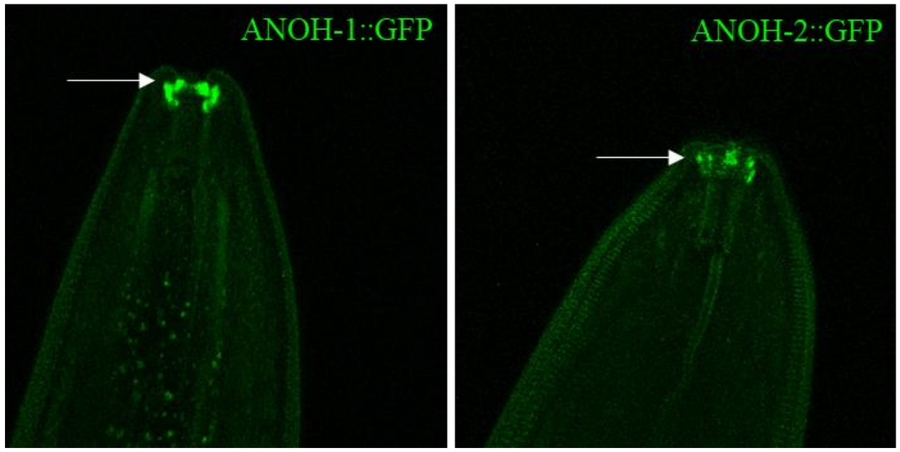

Figure 15: ANOH-1::GFP and ANOH-2::GFP localize to the cilia of the hermaphrodite head ciliated sensory neurons. Arrows indicate location of the cilia.

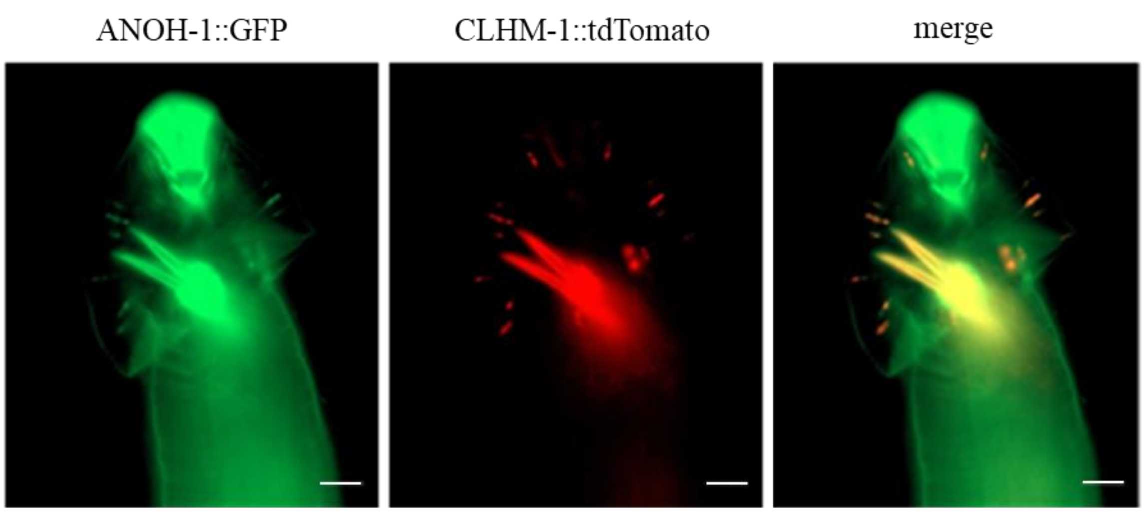

Figure 16: ANOH-1::GFP localizes to the cilia of the RnB ciliated sensory neurons.

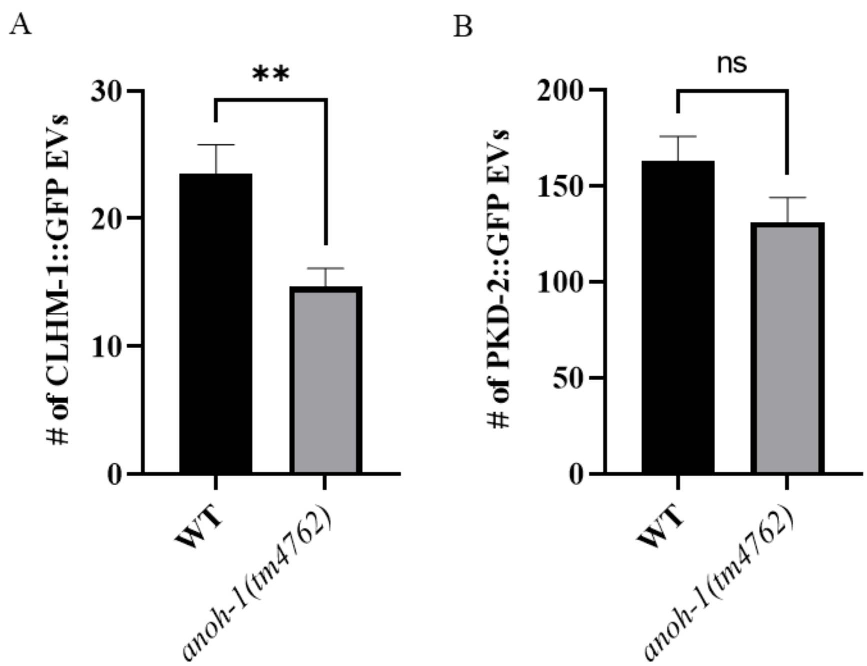

Figure 17: ANOH-1 plays a role in the biogenesis of CLHM-1 containing EVs but not PKD-2 EVs. (A) The number of CLHM-1::GFP EVs decreased significantly in the *anoh-1* animals compared to the control. (B) Loss of *anoh-1* did not result in a significant change in the amount of PKD-2::GFP EVs released.

3.7 The calcium ionophore ionomycin causes an increase in the release of CLHM-1 containing EVs

Ca^{2+} has been suggested to play an important role in MV release. ANOH-1 and ANOH-2 likely function as Ca^{2+}-dependent scramblases, translocating lipids upon stimulation by Ca^{2+} [85]. However, changes in EV release related to Ca^{2+} may be dependent on additional mechanisms. To investigate the role of Ca^{2+} on EV subpopulations released from the ciliated sensory neurons in *C. elegans*, I utilized the Ca^{2+} ionophore ionomycin. Ionomycin causes an increase in intracellular Ca^{2+} via PM ion channels and activation of the phospholipase C controlled mechanisms of Ca^{2+} release from Ca^{2+} stores in the ER [87,88]. Analysis of images revealed that ionomycin induced increased CLHM-1::GFP containing EV release, causing approximately a 50% increase in observed EVs (**Figure 18**). Further investigation must be done to determine the mechanisms by which ionomycin results in an increase in EV release.

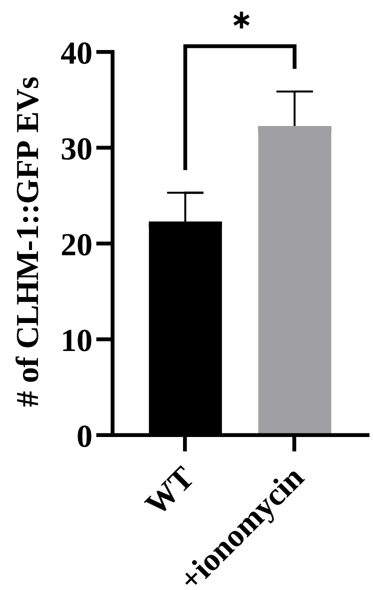

Figure 18: Ionomycin stimulates an increase in CLHM-1::GFP EV release from WT animals.

Chapter 4

DISCUSSION

Extracellular vesicles are released from all cell types and have proven themselves to be important disease markers, cellular communicators, treatment targets, and vehicles of drug delivery. As an abundance of research continues to support their critical roles in biological processes, more work is needed to understand the factors that control cargo sorting and biogenesis. Up until this point, progress in these areas of EV research has been severely limited by a reliance on primarily *in vitro* models. Utilization of the *C. elegans* ciliated sensory neurons as an *in vivo* EV model provides many important windows into studying EV biogenesis and cargo sorting.

Discovery of CLHM-1 and PKD-2 occupying different EV subsets provided the tools to explore the question of how cargoes that do colocalize in the cilia are sorted into EV subpopulations. We have provided multiple lines of evidence suggesting that spatial organization of cargo proteins within the cilia is a major mechanism of EV cargo sorting into separate populations. CLHM-1::tdTomato does not localize to the ciliary distal segment as seen when co-expressed with CIL-7::GFP, CHE-3::GFP and PKD-2::GFP. Instead, CLHM-1 can be seen within the middle segment and the PCMC, being barred also from the transition zone. On the other hand, PKD-2 is consistently transported to the ciliary tip as demonstrated by visual observation and in the two-dimensional analysis of fluorescence intensity peaks in the distal region. This was further supported by colocalization analysis, which revealed that there are many isolated areas where the fluorophores occupy distinct regions within the cilia and PCMC.

Anterograde motors affect cargo proteins differently. Transport of PKD-2 to the distal region is carried out redundantly by the homomeric OSM-3 motor and the heterotrimeric kinesin-2, evidenced by the correct localization of PKD-2 to the distal tip in either *osm-3* or *klp-11* animals. However, loss of *klp-11* does impact localization of cargo proteins, as seen in the changes in the Mander's coefficients compared to wild type. In both the cilia proper and the PCMC, loss of *klp-11* resulted in an increased percentage of GFP pixels colocalized with tdTomato pixels, and a decrease of tdTomato pixels overlapping with GFP. This could result from either a change in relative abundance of these proteins, with a decrease in CLHM-1 and increase in PKD-2 being most likely based on the data, or a change in localization. Additionally, loss of KLP-11 results in a decrease in CLHM-1 intensity in the PCMC, further suggesting a decrease in CLHM-1 abundance.

When PKD-2 is barred from entering the distal ciliary tip by complete disruption of anterograde transport as seen in the *klp-11;osm-3* double mutant a dramatic decrease in PKD-2 EV release is observed. This implies that a large portion of the PKD-2 only EVs were budding from the ciliary tip while colocalized EVs have a different point of origin, such as the PCMC or the middle segment. While PKD-2 relies on anterograde IFT for proper ciliary localization for packaging into EVs, CLHM-1 EV release and ciliary localization is independent of anterograde transport. However, a decrease in CLHM-1 intensity and colocalization is seen in the PCMC of single and double mutants of IFT anterograde transport, supporting the idea that retrograde transport is important for concentrating CLHM-1 within the PCMC.

Visual inspection of RnB neurons from CLHM-1::tdTomato; PKD-2::GFP animals showed no other consistent non-overlapping areas besides the distal tip, but instead the appearance of relatively high colocalization throughout the cilium proper and PCMC. Those highly colocalized areas likely give rise to separate subpopulations of EVs (CLHM-1 only, PKD-2 only and colocalized) via microdomains. Quantitative colocalization analysis of CLHM-1::tdT; PKD-2::GFP animals revealed that the areas that appeared highly colocalized were in reality significantly lower in percentage of overlapping pixels when compared to the CLHM-1::GFP; CLHM-1::tdTomato control. This supports the idea that within these largely colocalized areas are small specifically sorted regions that give rise to different EV subsets.

Disruption of the transition zone gate system for controlling cargo transportation from the PCMC to the cilia via the *mks-5(ok3582)* mutation resulted in a notable change in cilia and tail morphology, with cilia appearing shorter and less partitioned than normal cilia. This significant morphological change is not observed in the *mks-5(tm3100)* mutant, which takes out only a single isoform of MKS-5 (data not shown). *mks-5(ok3582)* results in a deletion that disrupts both isoforms, specifically the region between the Ca^{2+} sensing domains, but the reading frame is not disrupted so it may not fully knock-out protein function. EVs released from *mks-5(ok3582)* animals displayed an increase in the number of colocalized EVs (M. Clupper, personal communication). A significant increase in the percentage of GFP that colocalized with tdTomato was observed in the cilia and PCMC of *mks-5(ok3582)* animals. This increased colocalization could begin to explain the increased number of colocalized EVs released. Interestingly, this increase in colocalization is not observed in *mks-5(tm3100)*. Instead, there is a decrease in PKD-2::GFP EV release. This could be due to loss of the transition zone in this mutant which enables PIP2 to enter the cilia proper as an increase in PIP2 may reduce EV release[77]. Future experiments will be focused on determining how these two different alleles differentially impact EV release and colocalization. This will include ciliary analysis of the *mks-5(tm3100*) allele.

In addition to cargo sorting, our *C. elegans* EV model can be utilized to begin answering questions about EV biogenesis. Ionomycin stimulated increased CLHM-1 containing EV release. This could be via a calcium modulated scramblase or through regulation of another calcium-dependent step of microvesicle budding. The localization of calcium-dependent ANOH-1 and ANOH-2 to EV releasing cilia in the head, and ANOH-1 localization to the RnB neurons of the male tail suggested that these proteins might play a role in EV biogenesis. In my preliminary data, *anoh-1(tm4762)* reduced CLHM-EV release without significantly altering the release of PKD-2 EVs. Since these data were collected, subsequent imaging by another graduate student in the lab, Malek Elsayyid, produced contradictory data. This could be because the new data is more reliable due to our improved technique in imaging with the Andor Dragonfly with increased field of view and sensitivity or improved analysis protocol for quantifying EV release. Alternatively, we have discovered new information about how the presence of hermaphrodites on the same plate as males within the 24 hour before imaging significantly impacts EV release. The animals I imaged in the preliminary data were unmated, young adult males while all images collected by Malek were mated, young adult males. Future experiments with virgin males should be imaged using our improved EV sensitive imaging strategies to further investigate if ANOH-1 plays a role in EV biogenesis. Additionally, further examination is needed of the impact that animal density and ratio of males to hermaphrodites has on EV release in general to ensure proper controls for future EV imaging experiments.

The *C. elegans* EV model developed in the Tanis lab has allowed for many exciting opportunities to explore EV cargo and biogenesis mechanisms. This work has indicated that CLHM-1 and PKD-2 localization within the cilia is differentially controlled by anterograde IFT. Additionally, we have shown that localization of EV cargo to the distal segment, middle segment or PCMC can act as a mechanism for cargo sorting. It is likely that microdomains within these ciliary regions can also act as platforms for the biogenesis of specific EV subtypes in areas that are largely colocalized. The transition zone and proper cilia formation is also necessary for proper cargo loading into EVs. Finally, calcium-dependent scramblases and calcium signaling may play a role in microvesicle biogenesis of CLHM-1 containing EVs under certain conditions, although further research is needed to fully support this.

REFERENCES

1. Van Niel, G., D'Angelo, G. & Raposo, G. Shedding light on the cell biology of extracellular vesicles. *Nature Reviews Molecular Cell Biology* (2018) doi:10.1038/nrm.2017.125.
2. Lee, Y., El Andaloussi, S. & Wood, M. J. A. Exosomes and microvesicles: Extracellular vesicles for genetic information transfer and gene therapy. *Human Molecular Genetics* (2012) doi:10.1093/hmg/dds317.
3. El Andaloussi, S., Mäger, I., Breakefield, X. O. & Wood, M. J. A. Extracellular vesicles: Biology and emerging therapeutic opportunities. *Nature Reviews Drug Discovery* (2013) doi:10.1038/nrd3978.
4. Pollet, H., Conrard, L., Cloos, A. S. & Tyteca, D. Plasma membrane lipid domains as platforms for vesicle biogenesis and shedding? *Biomolecules* vol. 8 (2018).
5. Yuana, Y., Sturk, A. & Nieuwland, R. Extracellular vesicles in physiological and pathological conditions. *Blood Reviews* (2013) doi:10.1016/j.blre.2012.12.002.
6. E CHARGAFF, R. W. The biological significance of the thromboplastic protein of blood - PubMed. *J Biol Chem* **Nov;166**, 189–97 (1946).
7. De Broe, M. E., Wieme, R. J., Logghe, G. N. & Roels, F. Spontaneous shedding of plasma membrane fragments by human cells in vivo and in vitro. *Clinica Chimica Acta* **81**, 237–245 (1977).
8. Raposo, G. & Stoorvogel, W. Extracellular vesicles: Exosomes, microvesicles, and friends. *Journal of Cell Biology* vol. 200 373–383 (2013).
9. Lv, L. L., Feng, Y., Tang, T. T. & Liu, B. C. New insight into the role of extracellular vesicles in kidney disease. *Journal of Cellular and Molecular Medicine* vol. 23 731–739 (2019).
10. Nager, A. R. *et al.* An Actin Network Dispatches Ciliary GPCRs into Extracellular Vesicles to Modulate Signaling Article An Actin Network Dispatches Ciliary GPCRs into Extracellular Vesicles to Modulate Signaling. *Cell* **168**, 252–263 (2017).
11. Phua, S. C. *et al.* Dynamic remodeling of membrane composition drives cell cycle through primary cilia excision. *Cell* **168**, 264 (2017).
12. Mulcahy, L. A., Pink, R. C. & Carter, D. R. F. Routes and mechanisms of extracellular vesicle uptake. *Journal of Extracellular Vesicles* vol. 3 (2014).
13. Turturici, G., Tinnirello, R., Sconzo, G. & Geraci, F. Extracellular membrane vesicles as a mechanism of cell-to-cell communication: Advantages and

disadvantages. *American Journal of Physiology - Cell Physiology* vol. 306 621–633 (2014).
14. Hogan, M. C. *et al.* Characterization of PKD protein-positive exosome-like vesicles. *Journal of the American Society of Nephrology* **20**, 278–288 (2009).
15. Pan, B. T., Teng, K., Wu, C., Adam, M. & Johnstone, R. M. Electron microscopic evidence for externalization of the transferrin receptor in vesicular form in sheep reticulocytes. *Journal of Cell Biology* **101**, 942–948 (1985).
16. Wu, N. *et al.* Critical Role of Lipid Scramblase TMEM16F in Phosphatidylserine Exposure and Repair of Plasma Membrane after Pore Formation. *Cell Reports* **30**, 1129-1140.e5 (2020).
17. György, B. *et al.* Membrane vesicles, current state-of-the-art: Emerging role of extracellular vesicles. *Cellular and Molecular Life Sciences* vol. 68 2667–2688 (2011).
18. Sedgwick, A. E. & D'Souza-Schorey, C. The biology of extracellular microvesicles. *Traffic* vol. 19 319–327 (2018).
19. Akers, J. C., Gonda, D., Kim, R., Carter, B. S. & Chen, C. C. Biogenesis of extracellular vesicles (EV): Exosomes, microvesicles, retrovirus-like vesicles, and apoptotic bodies. *Journal of Neuro-Oncology* vol. 113 1–11 (2013).
20. Akers, J. C., Gonda, D., Kim, R., Carter, B. S. & Chen, C. C. Biogenesis of extracellular vesicles (EV): Exosomes, microvesicles, retrovirus-like vesicles, and apoptotic bodies. *Journal of Neuro-Oncology* vol. 113 1–11 (2013).
21. Johnsen, K. B., Gudbergsson, J. M., Andresen, T. L. & Simonsen, J. B. What is the blood concentration of extracellular vesicles? Implications for the use of extracellular vesicles as blood-borne biomarkers of cancer. *Biochimica et Biophysica Acta - Reviews on Cancer* (2019) doi:10.1016/j.bbcan.2018.11.006.
22. Nomura, S. Extracellular vesicles and blood diseases. *International Journal of Hematology* (2017) doi:10.1007/s12185-017-2180-x.
23. Berckmans, R. J. *et al.* Cell-derived microparticles circulate in healthy humans and support low grade thrombin generation. *Thrombosis and Haemostasis* (2001) doi:10.1055/s-0037-1615646.
24. Khan, M. M. H., Hattori, T., Niewiarowski, S., Edmunds, L. H. & Colman, R. W. Truncated and microparticle-free soluble tissue factor bound to peripheral monocytes preferentially activate factor VII. *Thrombosis and Haemostasis* (2006) doi:10.1160/TH05-06-0432.
25. Nomura, S. *et al.* High-shear-stress-induced activation of platelets and microparticles enhances expression of cell adhesion molecules in THP-1 and endothelial cells. *Atherosclerosis* (2001) doi:10.1016/S0021-9150(01)00433-6.
26. Gildea, J. J. *et al.* Exosomal transfer from human renal proximal tubule cells to distal tubule and collecting duct cells. *Clinical Biochemistry* **47**, 89–94 (2014).
27. Hogan, M. C. *et al.* Characterization of PKD protein-positive exosome-like vesicles. *Journal of the American Society of Nephrology* **20**, 278–288 (2009).

28. Lea, W. A. *et al.* Analysis of the polycystin complex (PCC) in human urinary exosome–like vesicles (ELVs). *Scientific Reports* (2020) doi:10.1038/s41598-020-58087-3.
29. Budnik, V., Ruiz-Cañada, C. & Wendler, F. Extracellular vesicles round off communication in the nervous system. *Nature Reviews Neuroscience* (2016) doi:10.1038/nrn.2015.29.
30. Goldie, B. J. *et al.* Activity-associated miRNA are packaged in Map1b-enriched exosomes released from depolarized neurons. *Nucleic Acids Research* (2014) doi:10.1093/nar/gku594.
31. Soria, F. N. *et al.* Exosomes, an unmasked culprit in neurodegenerative diseases. *Frontiers in Neuroscience* vol. 11 (2017).
32. Extracellular vesicles in physiological and pathological conditions | Elsevier Enhanced Reader. https://reader.elsevier.com/reader/sd/pii/S0268960X12000768?token=3D53FC4FBE91C8E577E61D56BFD06CDEF8211F6F517806635BD65CB386C56870A31EA4DF397ECD146B9524C581E8255E.
33. Han, L., Lam, E. W. F. & Sun, Y. Extracellular vesicles in the tumor microenvironment: Old stories, but new tales. *Molecular Cancer* vol. 18 1–14 (2019).
34. Janowska-Wieczorek, A. *et al.* Microvesicles derived from activated platelets induce metastasis and angiogenesis in lung cancer. *International Journal of Cancer* **113**, 752–760 (2005).
35. Skog, J. *et al.* Glioblastoma microvesicles transport RNA and proteins that promote tumour growth and provide diagnostic biomarkers. *Nature Cell Biology* **10**, 1470–1476 (2008).
36. Lucchetti, D., Tenore, C. R., Colella, F. & Sgambato, A. Extracellular vesicles and cancer: A focus on metabolism, cytokines, and immunity. *Cancers* (2020) doi:10.3390/cancers12010171.
37. Tang, Y. *et al.* The Biogenesis, Biology, and Clinical Significance of Exosomal PD-L1 in Cancer. *Frontiers in Immunology* vol. 11 604 (2020).
38. Pardoll, D. M. The blockade of immune checkpoints in cancer immunotherapy. *Nature Reviews Cancer* (2012) doi:10.1038/nrc3239.
39. Chen, D. S. & Mellman, I. Oncology meets immunology: The cancer-immunity cycle. *Immunity* (2013) doi:10.1016/j.immuni.2013.07.012.
40. Bricogne, C. *et al.* TMEM16F activation by Ca2+ triggers plasma membrane expansion and directs PD-1 trafficking. *Scientific Reports* (2019) doi:10.1038/s41598-018-37056-x.
41. Pollet, H., Conrard, L., Cloos, A. S. & Tyteca, D. Plasma membrane lipid domains as platforms for vesicle biogenesis and shedding? *Biomolecules* vol. 8 (2018).
42. Wu, K., Xing, F., Wu, S. Y. & Watabe, K. Extracellular vesicles as emerging targets in cancer: Recent development from bench to bedside. *Biochimica et Biophysica Acta - Reviews on Cancer* vol. 1868 538–563 (2017).

43. Yaari, Z. *et al.* Theranostic barcoded nanoparticles for personalized cancer medicine. *Nature Communications* **7**, 13325–13325 (2016).
44. Taylor, J. & Bebawy, M. Proteins Regulating Microvesicle Biogenesis and Multidrug Resistance in Cancer. *PROTEOMICS* **19**, 1800165 (2019).
45. Taylor, J. & Bebawy, M. Proteins Regulating Microvesicle Biogenesis and Multidrug Resistance in Cancer. *Proteomics* (2019) doi:10.1002/pmic.201800165.
46. Allan, D. & Michell, R. H. Calcium ion-dependent diacylglycerol accumulation in erythrocytes is associated with microvesiculation but not with efflux of potassium ions. *Biochemical Journal* **166**, 495–499 (1977).
47. Visser, D. *et al.* TRPM7 triggers Ca2+ sparks and invadosome formation in neuroblastoma cells. *Cell Calcium* (2013) doi:10.1016/j.ceca.2013.09.003.
48. Goll, D. E., Thompson, V. F., Li, H., Wei, W. & Cong, J. The calpain system. *Physiological Reviews* (2003) doi:10.1152/physrev.00029.2002.
49. Taylor, J., Jaiswal, R. & Bebawy, M. Calcium-calpain Dependent Pathways Regulate Vesiculation in Malignant Breast Cells. *Current Cancer Drug Targets* (2016) doi:10.2174/1568009616666161026165736.
50. Leventis, P. A. & Grinstein, S. The distribution and function of phosphatidylserine in cellular membranes. *Annual Review of Biophysics* vol. 39 407–427 (2010).
51. Bricogne, C. *et al.* TMEM16F activation by Ca2+ triggers plasma membrane expansion and directs PD-1 trafficking. *Scientific Reports* (2019) doi:10.1038/s41598-018-37056-x.
52. Bevers, E. M., Comfurius, P. & Zwaal, R. F. A. Changes in membrane phospholipid distribution during platelet activation. *BBA - Biomembranes* (1983) doi:10.1016/0005-2736(83)90169-4.
53. Janas, A. M., Sapoń, K., Janas, T., Stowell, M. H. B. & Janas, T. Exosomes and other extracellular vesicles in neural cells and neurodegenerative diseases. *Biochimica et Biophysica Acta - Biomembranes* vol. 1858 1139–1151 (2016).
54. Kastelowitz, N. & Yin, H. Exosomes and microvesicles: Identification and targeting by particle size and lipid chemical probes. *ChemBioChem* vol. 15 923–928 (2014).
55. Hankins, H. M., Baldridge, R. D., Xu, P. & Graham, T. R. Role of Flippases, Scramblases and Transfer Proteins in Phosphatidylserine Subcellular Distribution. *Traffic* (2015) doi:10.1111/tra.12233.
56. Bratton, D. L. *et al.* Appearance of phosphatidylserine on apoptotic cells requires calcium- mediated nonspecific flip-flop and is enhanced by loss of the aminophospholipid translocase. *Journal of Biological Chemistry* (1997) doi:10.1074/jbc.272.42.26159.
57. Falzone, M. E., Malvezzi, M., Lee, B. C. & Accardi, A. Known structures and unknown mechanisms of TMEM16 scramblases and channels. *Journal of General Physiology* (2018) doi:10.1085/jgp.201711957.

58. Yang, H. *et al.* TMEM16F forms a Ca2+-activated cation channel required for lipid scrambling in platelets during blood coagulation. *Cell* (2012) doi:10.1016/j.cell.2012.07.036.
59. Shukla, S., Jin, R., Robustelli, J., Zimmerman, Z. E. & Baumgart, T. PIP2 Reshapes Membranes through Asymmetric Desorption. *Biophysical Journal* (2019) doi:10.1016/j.bpj.2019.07.047.
60. Wang, J. & Barr, M. M. Ciliary Extracellular Vesicles: Txt Msg Organelles. *Cellular and Molecular Neurobiology* (2016) doi:10.1007/s10571-016-0345-4.
61. Williams, C. L. *et al.* MKS and NPHP modules cooperate to establish basal body/transition zone membrane associations and ciliary gate function during ciliogenesis. *Journal of Cell Biology* (2011) doi:10.1083/jcb.201012116.
62. Nachury, M. V. How do cilia organize signalling cascades? *Philosophical Transactions of the Royal Society B: Biological Sciences* vol. 369 (2014).
63. Bae, Y. K. & Barr, M. M. Sensory roles of neuronal cilia: Cilia development, morphogenesis, and function in C. elegans. *Frontiers in Bioscience* **13**, 5959–5974 (2008).
64. Kaletta, T. & Hengartner, M. O. Finding function in novel targets: C. elegans as a model organism. *Nature Reviews Drug Discovery* vol. 5 387–399 (2006).
65. Wang, J. *et al.* C. elegans ciliated sensory neurons release extracellular vesicles that function in animal communication. *Current Biology* **24**, 519–525 (2014).
66. Prevo, B., Scholey, J. M. & Peterman, E. J. G. Intraflagellar Transport: Mechanisms of Motor Action, Cooperation and Cargo Delivery. *The FEBS journal* **284**, 2905 (2017).
67. Wang, J. *et al.* Sensory cilia act as a specialized venue for regulated extracellular vesicle biogenesis and signaling. *Current Biology* **31**, (2021).
68. Wang, J., Nikonorova, I. A., Gu, A., Sternberg, P. W. & Barr, M. M. Release and targeting of polycystin-2-carrying ciliary extracellular vesicles. *Current Biology* vol. 30 R755–R756 (2020).
69. Maguire, J. E. *et al.* Myristoylated CIL-7 regulates ciliary extracellular vesicle biogenesis. **26**, (2015).
70. O'Hagan, R. *et al.* Glutamylation Regulates Transport, Specializes Function, and Sculpts the Structure of Cilia. *Current Biology* (2017) doi:10.1016/j.cub.2017.09.066.
71. Clupper, M. *et al.* Kinesin-II motors differentially impact biogenesis of distinct extracellular vesicle subpopulations shed from C. elegans sensory cilia. *bioRxiv* 2021.12.19.473369 (2021) doi:10.1101/2021.12.19.473369.
72. Yi, P., Li, W. J., Dong, M. Q. & Ou, G. Dynein-Driven Retrograde Intraflagellar Transport Is Triphasic in C. elegans Sensory Cilia. *Current Biology* (2017) doi:10.1016/j.cub.2017.04.015.
73. Morsci, N. S. & Barr, M. M. Kinesin-3 KLP-6 regulates intraflagellar transport in male-specific cilia of Caenorhabditis elegans. *Current biology : CB* **21**, 1239 (2011).

74. Evans, J. E. *et al.* Functional modulation of IFT kinesins extends the sensory repertoire of ciliated neurons in Caenorhabditis elegans. *The Journal of cell biology* **172**, 663–669 (2006).
75. Mukhopadhyay, S. *et al.* Distinct IFT mechanisms contribute to the generation of ciliary structural diversity in C. elegans. *The EMBO Journal* **26**, 2966–2980 (2007).
76. Snow, J. J. *et al.* Two anterograde intraflagellar transport motors cooperate to build sensory cilia on C. elegans neurons. *Nature cell biology* **6**, 1109–1113 (2004).
77. Jensen, V. L. *et al.* Formation of the transition zone by Mks5/Rpgrip1L establishes a ciliary zone of exclusion (CIZE) that compartmentalises ciliary signalling proteins and controls PIP 2 ciliary abundance . *The EMBO Journal* **34**, 2537–2556 (2015).
78. Li, C. *et al.* MKS5 and CEP290 Dependent Assembly Pathway of the Ciliary Transition Zone. *PLoS Biology* (2016) doi:10.1371/journal.pbio.1002416.
79. Wehman, A. M., Poggioli, C., Schweinsberg, P., Grant, B. D. & Nance, J. The P4-ATPase TAT-5 inhibits the budding of extracellular vesicles in C. elegans embryos. *Current Biology* (2011) doi:10.1016/j.cub.2011.10.040.
80. Li, Z. *et al.* Necrotic Cells Actively Attract Phagocytes through the Collaborative Action of Two Distinct PS-Exposure Mechanisms. *PLoS Genetics* **11**, (2015).
81. Skotland, T., Sagini, K., Sandvig, K. & Llorente, A. An emerging focus on lipids in extracellular vesicles. *Advanced Drug Delivery Reviews* (2020) doi:10.1016/j.addr.2020.03.002.
82. Skotland, T., Sandvig, K. & Llorente, A. Lipids in exosomes: Current knowledge and the way forward. *Progress in Lipid Research* (2017) doi:10.1016/j.plipres.2017.03.001.
83. Malvezzi, M. *et al.* Out-of-the-groove transport of lipids by TMEM16 and GPCR scramblases. *Proceedings of the National Academy of Sciences of the United States of America* (2018) doi:10.1073/pnas.1806721115.
84. Furuta, Y., Pena Ramos, O., Li, Z. & Zhou, Z. Calcium ions trigger the exposure of phosphatidylserine on the surface of necrotic cells. *bioRxiv* (2020) doi:https://doi.org/10.1101/2020.08.21.260695.
85. Wang, Y. *et al.* Phylogenetic, expression, and functional analyses of anoctamin homologs in Caenorhabditis elegans. *American Journal of Physiology - Regulatory Integrative and Comparative Physiology* (2013) doi:10.1152/ajpregu.00303.2012.
86. Hodgkin, J., Horvitz, H. R. & Brenner, S. Nondisjunction Mutants of the Nematode CAENORHABDITIS ELEGANS. *Genetics* (1979).
87. Dedkova, E. N., Sigova, A. A. & Zinchenko, V. P. Mechanism of action of calcium ionophores on intact cells: Ionophore-resistant cells. *Membrane and Cell Biology* (2000).

88. Chatila, T., Silverman, L., Miller, R. & Geha, R. Mechanisms of T cell activation by the calcium ionophore ionomycin. *Journal of immunology (Baltimore, Md. : 1950)* (1989).